



Cite this: DOI: 10.1039/d5gc01721a

## Enhancing *Verbena officinalis* L. antioxidant yield through natural deep eutectic solvents and MOF synergistic application†

 Haixiang Li,  ‡<sup>a,b,c</sup> Kunze Du,  ‡<sup>b,c</sup> Chong Liu,  <sup>d</sup> Yumin Yang,<sup>a,b,c</sup> Cailin Ye,<sup>a,b,c</sup> Xiaoxia Li  \*<sup>a,b,c</sup> and Yanxu Chang\*<sup>b,c</sup>

The bioactive components in *Verbena officinalis* L. extract have been demonstrated to exhibit remarkable pharmacological properties. However, the active ingredients obtained by organic solvent extraction posed a challenge to their application. In this research, a method was proposed for extracting the active ingredient from *Verbena officinalis* L., in which MOFs were used as adsorbents and natural eutectic solvents (NADESS) as additives in water. The synthetic MOF with a high surface area and porous structure could disrupt the cell walls and adsorb the target components from the herb. Meanwhile, the abundant hydrogen bonding system and polarity adjustability of NADESS enhanced the dissolution of active ingredients. After optimization, the total extraction efficiency of five target substances could reach  $22.99 \pm 0.67$  mg g<sup>-1</sup> by using only 1.52% NADES aqueous solution, and the antioxidant capacity of the extracts was better than that of traditional extraction methods. Additionally, density functional theory revealed that NADESS interacted with the active ingredient through hydrogen bonding, enhancing its dissolution and protecting the active site before it exerted its antioxidant power. The NADES dosage was proven to be the most important factor in the extraction process through machine learning, and a Graphical User Interface model was developed to predict the yield based on input variables. Batch experiments proved that *Verbena officinalis* L. extracts from different sources were suitable for the technology proposed in this work. This technology utilized the synergistic effect of NADESS and MOFs, thereby not only minimizing solvent costs and eliminating the need for solvent recovery but also demonstrating global application value and fully implementing the green concept.

Received 8th April 2025,

Accepted 12th May 2025

DOI: 10.1039/d5gc01721a

[rsc.li/greenchem](https://rsc.li/greenchem)

### Green foundation

1. This work introduces a more sustainable extraction strategy using natural deep eutectic solvents (NADESS) as trace additives in water. Through hydrogen bonding, NADESS enhanced the antioxidant properties of *Verbena officinalis* L., while their ultra-low dosage eliminated the need for solvent recovery. This design provides a green and practical formulation for herbal enrichment.
2. A more sustainable extraction and enrichment method has been achieved, significantly enhancing the antioxidant capacity of *Verbena officinalis* L. by identifying 3 flavonoids, 3 iridoids, and 4 phenylethanoid glycosides within it.
3. Future work will focus on screening more efficient NADES formulations to boost additional pharmacological activities of herbal products, such as anti-inflammatory, neuroprotective, and immunomodulatory effects.

## 1. Introduction

*Verbena officinalis* L. is a common natural product (NP) of the genus *Verbena officinalis* L in the verbena family.<sup>1</sup> The primary bioactive components of *Verbena officinalis* L. include iridoids, phenylethanoid glycosides, essential oil, flavonoids and so on, which exhibit various pharmacological activities such as antioxidant, antitumor, and antimicrobial effects.<sup>2–4</sup> Among them, antioxidant components can remove free radicals and delay aging, which have attracted wide attention.<sup>5</sup> However, conventional extraction methods often rely on organic solvents, such

<sup>a</sup>School of Chinese Materia Medica, Tianjin University of Traditional Chinese Medicine, Tianjin, 301617, China. E-mail: lixx@tjutcm.edu.cn, Tcmcyx@tjutcm.cn

<sup>b</sup>State Key Laboratory of Chinese Medicine Modernization, Tianjin University of Traditional Chinese Medicine, Tianjin, 301617, China

<sup>c</sup>Tianjin Key Laboratory of Therapeutic Substance of Traditional Chinese Medicine, Tianjin University of Traditional Chinese Medicine, Tianjin, 301617, China

<sup>d</sup>Department of Chemical & Materials Engineering, University of Auckland, Auckland, 0926, New Zealand

† Electronic supplementary information (ESI) available. See DOI: <https://doi.org/10.1039/d5gc01721a>

‡ These authors contributed equally to this work.

as ethanol<sup>6</sup> and methanol,<sup>7</sup> which are not only toxic to humans but also cause pollution to the environment. Additional steps like solvent recovery, purification, and compliance checks are also needed, making the process more complex and expensive. In addition, such solvents are often utilized in conjunction with heating extraction, resulting in high energy consumption and the unintended dissolution of a substantial number of impurities. Therefore, it is imperative that a method be developed that uses green and highly efficient solvents together with highly selective pre-treatment techniques to extract antioxidant components from *Verbena officinalis* L.

As a new kind of green solvent, deep eutectic solvents (DESS) were proposed by the Abbott team in 2003,<sup>8</sup> which have the advantages of low cost, low toxicity, a simple preparation process, being non-flammable and high stability.<sup>9</sup> These solutions are homogeneous and clarified, resulting from the continuous stirring of hydrogen bond donor (HBD) and hydrogen bond acceptor (HBA) components at elevated temperatures, facilitated by hydrogen bonding interactions.<sup>10</sup> Natural deep eutectic solvents (NADESs) are defined as solvents composed of primary or secondary metabolites that are sourced from living organisms. These metabolites may include sugars, amino acids, organic acids, fatty acids, or chlorine derivatives. Such solvents exhibit enhanced biocompatibility and are considered more environmentally sustainable.<sup>11</sup> Since Choi *et al.* used NADESs as an alternative solvent in 2011,<sup>12</sup> the use of NADESs to extract NPs has attracted increasing attention. Owing to their rich hydrogen bond system and polarity adjustability, NADESs have high solubility for bioactive components, which has made them regarded as novel ideal solvents by the scientific community.<sup>13</sup> For example, Zuo *et al.*<sup>14</sup> used 20 NADESs to extract flavonoids from *Trollius ledebourii*. Bajkacz *et al.*<sup>15</sup> utilized 17 NADESs for the isolation of isoflavones (daidzin, genistin, genistein and daidzein) from soy products. However, even though NADESs are green solvents, using them as extraction solutions is not only costly, but their poor volatility also makes them difficult to recover.<sup>16</sup> Therefore, there is a need to develop a cost-effective technology for extracting the active ingredients in NPs using NADESs, which can avoid the recycling of NADESs at the same time.

Matrix solid-phase dispersion (MSPD) is a sample pretreatment method appropriate for semi-solid, solid and viscous samples.<sup>17</sup> In MSPD, the sample and the adsorbent are fully mixed by grinding, and then the solid mixture is eluted with an elution solution, while the target compound is separated, extracted and purified from the solution, simplifying the procedure.<sup>18</sup> Several studies have reported the use of modified MSPD techniques for extracting active ingredients from NPs. For instance, Wang *et al.*<sup>19</sup> and Xu *et al.*<sup>20</sup> utilized ultrasound-assisted MSPD (UA-MSPD) to extract active ingredients from *Hibiscus sabdariffa* L. and *Fructus Choerospondias*, respectively. Wen *et al.*<sup>21</sup> applied vortex-assisted MSPD (VA-MSPD) to extract bioactive compounds from *Paeoniae Radix Rubra*. The adsorbent in MSPD can help the sample to be evenly dispersed on the surface of the adsorbent during the grinding process and

selectively adsorb the target object to reduce the interference of impurities.<sup>22</sup> At present, the mainstream adsorbents mainly include silica gel, silica, molecular sieves and so on. As a kind of polymer crystal material formed by metal ions and organic ligands, MOFs were first synthesized by Yaghi in 1995.<sup>23</sup> Their high specific surface area, unique pore size and function make them widely used in adsorption and extraction fields.<sup>24</sup> For example, Hurley *et al.*<sup>25</sup> used the MOFs Al-PyrMOF and Zr-NU-1000 to recover bioactive berry NPs. Xiang *et al.*<sup>26</sup> utilized a neutral Cu-based MOF to extract quercetin from onion juice. Liu *et al.*<sup>27</sup> used a PU/GO/BA-MOF composite to adsorb *cis*-diol from peanut shells. Therefore, the high absorbability and selectivity of MOFs can make them a reliable adsorbent for the MSPD process.

Machine learning (ML) is a technique that uses algorithms and statistical models to enable computers to make predictions or decisions.<sup>28</sup> At present, common algorithms include linear regression, random forest, and gradient boosting trees. Linear regression is fast in terms of training and prediction speed but struggles with complex nonlinear relationships. Random forest can handle large-scale datasets but incurs high computational and storage costs. Gradient boosting trees, a class of ensemble learning algorithms based on boosting, combine multiple weak learners into a strong learner to improve prediction accuracy and are highly cost-effective.<sup>29–31</sup> At present, ML has been widely used in many fields such as the electronics industry, materials science, medical treatment, separation and extraction.<sup>32–34</sup> In terms of separation and extraction, ML can monitor key process parameters in real time, such as temperature, pressure, and the flow rate. Based on changes in these parameters, it can adjust operating conditions to achieve process optimization and control. This approach helps improve production efficiency and reduce energy consumption and costs. For example, N. Taoufik *et al.*<sup>35</sup> used ML to predict the adsorption capacity of calcined Cu–Al layered double hydroxides for caffeine. Zhao *et al.*<sup>36</sup> utilized the ML model to rank 8 factors affecting the adsorption process and found the most important separation driving force. Although ML has not yet been used in the extraction process of NPs, it has significant reference value for the analysis of the MSPD pretreatment process of *Verbena officinalis* L.

This experiment was the first to propose combining MOFs and NADESs using the UA-MSPD method to extract the active ingredient from *Verbena officinalis* L. When the MOF was used as an adsorbent, its high specific surface area and porous structure could effectively destroy the cell wall, adsorb the target component and promote its dissolution. When NADES was used as a small additive, its hydrogen bond system and polarity could enhance the solubility of the solvent to the active ingredient. After a series of optimizations, the combination of an appropriate amount of MOF and an aqueous solution containing a small amount of NADES could achieve efficient extraction of the five target substances. The results of antioxidant tests proved that the extracted solution obtained by this method had better antioxidant activity than the tra-

ditional method, and the subsequent mass spectrometry identified the antioxidant components of the extract. After selecting the best model, machine learning was used to rank the influencing factors, reveal the variables with the highest weight, and develop a Graphical User Interface model to implement the input variables to predict the output. Finally, DFT was used to analyse the mechanism of action and the reason for its high antioxidant activity, providing a theoretical basis at the microscopic level. The experimental process is depicted in Fig. 1. This work demonstrated that using a small amount of NADES in combination with MOFs can promote the dissolution of active ingredients. This approach not only reduced solvent costs and eliminated the need for solvent recovery but also enhanced the application value of antioxidant components, showing promising potential for large-scale green production.

## 2. Materials and methods

### 2.1. Reagents and materials

Hastatoside ( $\geq 98\%$ ), cornin ( $\geq 98\%$ ), acteoside ( $\geq 98\%$ ), luteolin ( $\geq 98\%$ ) and apigenin ( $\geq 98\%$ ) were purchased from Chengdu Lemeitian Pharmaceutical Technology Co., Ltd (Chengdu, China). Choline chloride ( $\geq 98\%$ ), betaine ( $\geq 98\%$ ), D/L-lactic acid ( $\geq 98\%$ ), malic acid ( $\geq 98\%$ ), ascorbic acid ( $\geq 98\%$ ), glycerol ( $\geq 98\%$ ), propylene glycol ( $\geq 98\%$ ), trimeric acid ( $\geq 98\%$ ), *p*-phthalic acid ( $\geq 98\%$ ), *N,N*-dimethylformamide (DMF) ( $\geq 98\%$ ), copper(II) nitrate hydrate ( $\geq 98\%$ ), chromic nitrate nonahydrate ( $\geq 98\%$ ), hydrofluoric acid ( $\geq 98\%$ ), tetramethylammonium fluoride ( $\geq 98\%$ ), ferric chloride hexahydrate ( $\geq 98\%$ ), cobaltous nitrate hexahydrate ( $\geq 98\%$ ), 1,2-dimethylimidazole ( $\geq 98\%$ ), ethanol ( $\geq 98\%$ ), methanol ( $\geq 98\%$ ), 1,1-

diphenyl-2-picrylhydrazyl radical 2,2-diphenyl-1-(2,4,6-trinitrophenyl)hydrazyl (DPPH) ( $\geq 99\%$ ), 2,2'-azino-bis (3-ethylbenzothiazoline-6-sulfonic acid) (ABTS) ( $\geq 99\%$ ), potassium persulfate ( $\geq 98\%$ ), salicylic acid ( $\geq 98\%$ ), ferrous sulfate ( $\geq 98\%$ ), trichloroacetic acid ( $\geq 98\%$ ), potassium ferricyanide ( $\geq 98\%$ ) and phosphate buffered saline (PBS) ( $\geq 98\%$ ) were obtained from Shanghai Macklin Biochemical Technology Co., Ltd (Shanghai, China). Cleanert COOH, Cleanert C18 and Cleanert PWCX were purchased from Tianjin Agela & Phenomenex Technology Co., Ltd (Tianjin, China). Hydrogen peroxide (3%) was purchased from Shanghai Maokang Biotechnology Co., Ltd (Shanghai, China). Chromatographic grade acetonitrile and phosphoric acid were purchased from Tianjin Concord Technology Co., Ltd (Tianjin, China). Nile red dye was obtained from Shanghai Acme Biochemical Co., Ltd (Shanghai, China). Ultrapure water was obtained by using a Milli-Q machine (Billerica, USA).

Different batches of *Verbena officinalis* L. were obtained from Puning in Guangdong Province, Meizhou in Guangdong Province, Hebei Province, Anhui Province, Shanxi Province, Yunnan Province, Germany and France. Before using, the herbs were authenticated based on morphological characteristics. They were then dried and crushed using a mechanical grinder. The powder was passed through an 80-mesh sieve to obtain particles smaller than 180 micrometres. The sieved samples were stored in sealed containers at room temperature ( $\sim 25\text{ }^{\circ}\text{C}$ ) in a dark, ventilated environment for no longer than one month prior to use.

### 2.2. Preparation and screening of NADESs and MOFs

Based on the purpose of large-scale green production, economic factors were the main concern in our screening process. Choline chloride and betaine, as common natural HBDs, were

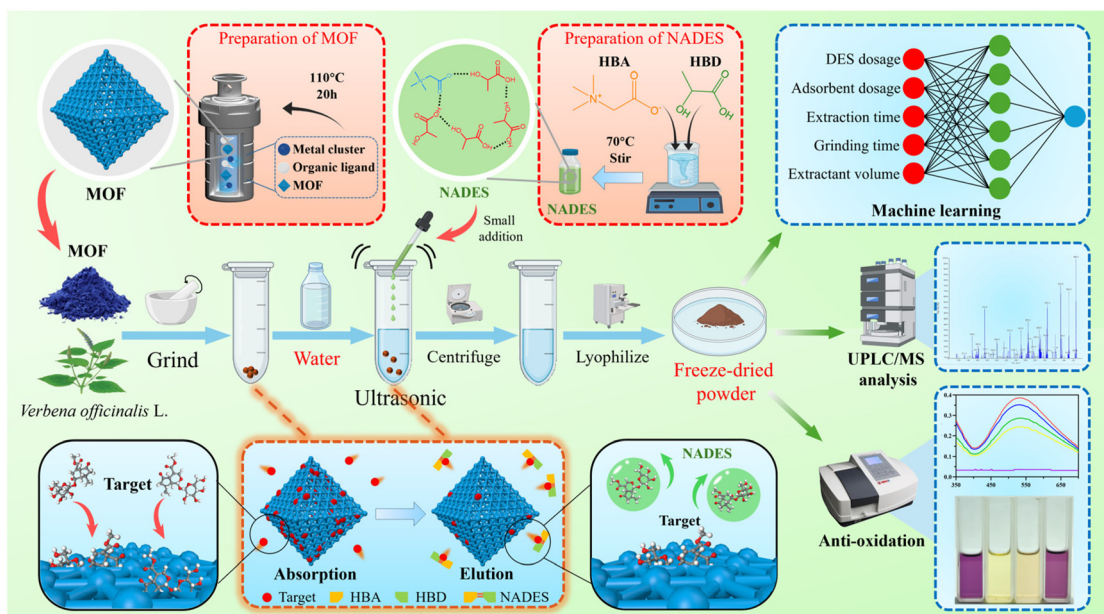


Fig. 1 Schematic diagram of the proposed extraction strategy and its application.

not only cheap and widely used, but also had many precedents for their use in the extraction of natural products.<sup>37,38</sup> Organic acids and polyols possess more hydrogen bonding sites, compared to other potential hydrogen bond donors or acceptors, due to their abundant carboxyl and hydroxyl groups. This high density of hydrogen bonding sites enhances the ability of the DES to form stable hydrogen bond networks and perform its function effectively. Therefore, five HBDs (malic acid, lactic acid, ascorbic acid, propylene glycol and glycerol) and two HBA (choline chloride and betaine) were selected to synthesize NADESs. They were placed in a round-bottomed flask according to the specified molar ratio and then heated and stirred simultaneously using a hotplate magnetic stirrer equipped with a thermocouple for temperature monitoring (maintained at 70 °C, 0.5–2 h, 1400 rpm) until a clear and homogeneous liquid was formed. A total of 32 types of NADESs (Table S1†) were synthesized in the experiment. After standing at room temperature for 12 hours to allow complete stabilization and to observe the physical properties, 8 NADESs were selected for follow-up experiments based on their characteristics of a uniform and transparent appearance, a stable state, and the absence of precipitates. They were betaine:lactic acid = 1:4 (Bet:Lac = 1:4), choline chloride:malic acid = 1:1 (ChCl:H<sub>2</sub>MA = 1:1), choline chloride:ascorbic acid = 2:1 (ChCl:Vit C = 2:1), choline chloride:lactic acid = 1:4 (ChCl:Lac = 1:4), betaine:propylene glycol = 1:4 (Bet:PG = 1:4), choline chloride:propylene glycol = 1:3 (ChCl:PG = 1:3), betaine:glycerol = 1:2 (Bet:Gl = 1:2) and choline chloride:glycerol = 1:2 (ChCl:Gl = 1:2); the above numbers are molar ratios. The appearance of NADESs is shown in Fig. 2a.

In view of the high specific surface area and abundant pore structure of MOF-199, the high adsorption selectivity of ZIF-67 for the target object in water, the high adsorption capacity of MIL-101 (Fe) for the removal of pollutants in water, and the good chemical inertia of MIL-101 (Cr) for complex systems, these four MOFs have become commonly used adsorbents in the adsorption field.<sup>39–42</sup> To compare the application of different types of MOFs in the extraction and separation of active components of NPs, they were selected as research objects in this experiment. Four kinds of MOFs were all synthesized by hydrothermal methods. The whole synthesis methods are given in the ESI.†

### 2.3. HPLC conditions

The analysis of herbal constituents was conducted utilizing an Agilent 1260 Infinity High-Performance Liquid Chromatography (HPLC) system, which was equipped with a diode array detector (Agilent, Santa Clara, USA). The chromatographic column employed was a Welch Ultimate AQ-C18 with the specifications of 5 μm particle size and dimensions of 4.6 × 250 mm. Detection wavelength: 238 nm; column temperature: 30 °C; flow rate: 1.0 mL min<sup>-1</sup>; injection volume: 10.00 μL; analysis time: 30 min; balance time: 5 min; mobile phase: 0.2% phosphoric acid solution (A) and acetonitrile (B); the corresponding gradient elution procedure was as follows: 0–15 min, 14%–30% (B); 15–24 min, 30%–47% (B); 24–30 min,

47%–48% (B). Under the above chromatographic conditions, all the target compounds achieved the best separation conditions. The chromatogram is shown in Fig. S1.†

### 2.4. Standard solution

Given that the main components in *Verbena officinalis* L. are iridoids, phenylethanol glycosides, and flavonoids, which exhibit antioxidant activities,<sup>43–45</sup> hastatoside (an iridoid), cornin (an iridoid), acteoside (a phenylethanol glycoside), luteolin (a flavonoid), and apigenin (a flavonoid) were selected as representative active ingredients. The total content of these five compounds was used as an index to optimize the extraction conditions.

The standards of hastatoside, cornin, acteoside, luteolin and apigenin were precisely weighed and then dissolved in methanol at the concentration of 3 mg mL<sup>-1</sup>, 2 mg mL<sup>-1</sup>, 2 mg mL<sup>-1</sup>, 1 mg mL<sup>-1</sup> and 1 mg mL<sup>-1</sup>, respectively. Subsequently, a specific volume of each standard solution was extracted and diluted with methanol to create a mixed standard solution with varying concentrations. All standard solutions were maintained at a temperature of 4 °C prior to utilization.

### 2.5. UA-MSPD

20.00 mg of Puning *Verbena officinalis* L. dry powder (sample) and 10.00 mg of MOF-199 powder (adsorbent) were weighed accurately and slowly poured into an agate mortar, and then ground fully with a grinding pestle clockwise for 2 min. The mixture was then transferred to a 5 mL centrifuge tube with 2.5 mL of water (eluent) containing 1% NADES (Bet:Lac = 1:4). After that, the solution was ultrasonically treated in a water bath for 7.5 min and centrifuged at 14 000 rpm for 5 min, and finally the supernatant was collected and filtered by using a 0.22 μm microporous filter membrane for HPLC analysis.

### 2.6. Extraction condition optimization

**2.6.1. Single factor optimization.** In order to find out the best conditions for extracting *Verbena officinalis* L. by a UA-MSPD method based on NADES and MOF, the following 7 factors affecting the extraction process were investigated in turn: adsorbent types (MOF-199, MIL-101(Cr), MIL-101(Fe), ZIF-67, COOH, C18 and PWCX), sample to adsorbent ratio (1:0, 2:1, 1:1 and 1:2), grinding time (1 min, 2 min, 3 min and 4 min), types of eluents (methanol, ethanol, water, Bet:Lac = 1:4, ChCl:H<sub>2</sub>MA = 1:1, ChCl:Vit C = 2:1, ChCl:Lac = 1:4, Bet:PG = 1:4, ChCl:PG = 1:3, Bet:Gl = 1:2 and ChCl:Gl = 1:2), DES dosage in water (0%, 1%, 2%, 3%, 4%, 5%, 6%, 8%, 10%, 12%, 15% and 50%), extractant volume (0.5 mL, 1 mL, 1.5 mL, 2 mL, 2.5 mL and 3 mL) and extraction time (2.5 min, 5 min, 7.5 min and 10 min). After determining the best conditions of one influencing factor, it was used to optimize the subsequent influencing factors until the best extraction conditions are found. All experiments were repeated three times.

**2.6.2. RSM optimization.** According to the findings derived from the single factor optimization experiment, adsorbent dosage (A: 0 mg, 10 mg and 20 mg), grinding time (B: 1 min,

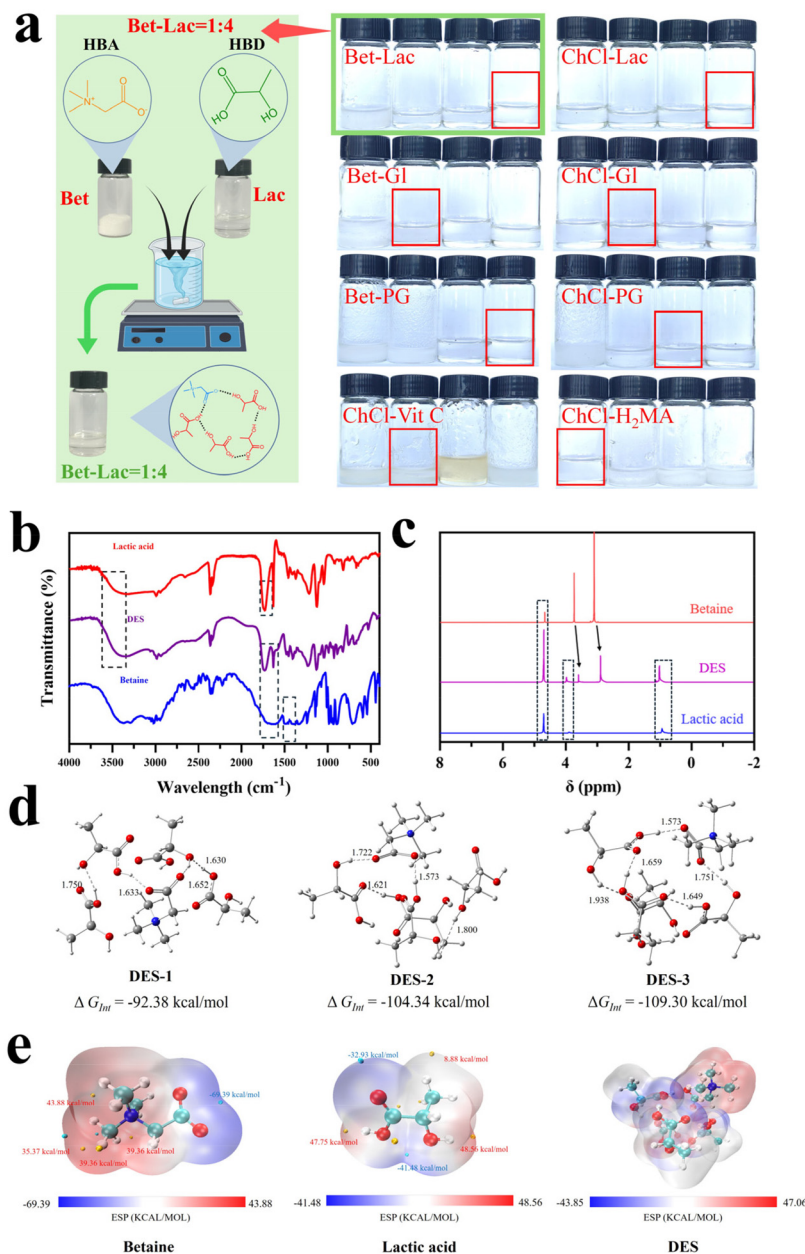


**Fig. 2** (a) Image of NADES and their synthesis process. (b) FT-IR spectroscopy of DES and its components. (c) <sup>1</sup>H NMR spectroscopy of DES and its components. (d)  $\Delta G_{int}$  of three different DES configurations. (e) ESP distribution of DES and its components.

2 min and 3 min), DES dosage ( $C$ : 0%, 1% and 2%), extractant volume ( $D$ : 2 mL, 2.5 mL and 3 mL) and extraction time ( $E$ : 5 min, 7.5 min and 10 min) were selected for the response surface methodology (RSM) optimization. 46 experiments of these parameters (5 factors and 3 levels) would be designed using a Box–Behnken design in Design Expert (version 13) (Table S2<sup>†</sup>).

## 2.7. Machine learning application

**2.7.1. Machine learning model construction.** Given the large-scale and nonlinearity of our dataset, the predictive performance of six machine learning models based on Boosting

Trees was compared using Python 3.13.1. Boosting Trees was a highly effective ensemble learning method that optimizes errors by iteratively combining multiple weak learners. It demonstrated high accuracy, flexibility, and excellent modeling ability for nonlinear relationships. Additionally, Boosting Trees performed exceptionally well in feature selection, handling imbalanced data, and controlling overfitting, while also supporting missing value handling and efficient implementation. Due to their wide application, the six models selected for this study included AdaBoost, CatBoost, GBDT, HistGB, LightGBM, and XGBoost. For a detailed introduction to the theoretical foundations of these models, refer to Table S3.<sup>†</sup>

The dataset collected through the Box–Behnken design was divided into training and testing sets in an 8:2 ratio. This study determined the optimal hyperparameters for each model by combining Bayesian optimization with grid search cross-validation (CV = 5). The selection range for the hyperparameters was based on previous literature as well as exploratory performance tests conducted on the machine learning data of this study.<sup>46</sup> The hyperparameters and their value ranges are also detailed in Table S3.†

The assessment of the model performance was conducted using two key metrics: Root Mean Squared Error (RMSE) and *R*-squared (*R*<sup>2</sup>). The formulas for calculating these metrics are presented in formulas (1) and (2), respectively. The model performance on the training and testing sets was quantitatively analysed using these two metrics.

$$\text{RMSE} = \sqrt{\frac{\sum_{i=1}^n (y_i - x_i)^2}{n}} \quad (1)$$

$$R^2 = 1 - \frac{\sum_{i=1}^n (y_i - x_i)^2}{\sum_{i=1}^n (y_i - \bar{y}_i)^2} \quad (2)$$

Here,  $y_i$  and  $x_i$  represented the predicted and experimental values, respectively. The symbol  $\bar{y}_i$  denoted the average of the experimental values, and  $n$  represented the total number of samples.

**2.7.2. Model interpretation.** To provide a comprehensive interpretation of the model, this study employed the SHapley Additive exPlanations (SHAP) analysis method in Python 3.13.1. SHAP values quantified the average contribution of each feature to the model's predictions and clearly indicated the impact of individual feature values on specific prediction outcomes. This method was particularly well-suited for analyzing the dynamics of complex tree models and identifying key features.

## 2.8. *In vitro* antioxidant test

After the supernatant was obtained by centrifugation, the antioxidant capacity of the UA-MSPD extract was compared with the ethanol extract. The antioxidant capacity of DES was determined separately through full wavelength scanning to exclude its effects. Ascorbic acid (Vit C) served as the positive control in tests. The MAPADA P9 ultraviolet–visible (UV–vis) spectrophotometer (Shanghai, China) was used to detect the absorbance of every concentration of the sample. Each detection procedure was repeated three times.

**2.8.1. DPPH radical scavenging test.** DPPH was commonly utilized to assess the free radical scavenging activity of samples in an alcoholic medium, where an antioxidant could convert it from purple to yellow. Based on this principle and previous research,<sup>47</sup> the experimental group (B), blank group (C), and control group (A) were evaluated for absorbance at 517 nm. The mixture was subjected to thorough agitation and subsequently incubated at 37 °C for a duration of 30 minutes in a dark environment before measurement. The concentration of the DPPH solution was established at 2 mmol L<sup>-1</sup>,

and the free radical scavenging rate was determined using formula (3):

$$\text{Scavenging rate (\%)} = [1 - (B - C)/A] \times 100\%, \quad (3)$$

where  $B$  represents the mixture of 200 μL of DPPH solution and 200 μL of sample solution.  $C$  indicates the mixture of 200 μL of sample solution and 200 μL of ethanol.  $A$  represents the mixture of 200 μL of DPPH solution and 200 μL of ethanol.

**2.8.2. ABTS radical scavenging test.** The ABTS stock solution was prepared by mixing ABTS and potassium persulfate at a molar ratio of approximately 2.86:1 (7 mmol L<sup>-1</sup> ABTS and 2.45 mmol L<sup>-1</sup> potassium persulfate) under dark conditions, leading to the formation of a dark green solution. The stock solution was then diluted 7-fold with ethanol to create the ABTS working solution. When the solution reacted with proton-donating hydrogen, the dark green color faded. Based on previous literature,<sup>48</sup> all mixtures were thoroughly shaken and allowed to stand at 37 °C for 10 minutes in a dark environment. Subsequently, the absorbance was assessed at a wavelength of 734 nm. The rate of ABTS free radical scavenging was determined utilizing formula (4):

$$\text{Scavenging rate (\%)} = [1 - (B - C)/A] \times 100\%, \quad (4)$$

where  $B$  represents the mixture of 200 μL of ABTS working solution and 200 μL of sample solution.  $C$  indicates the mixture of 200 μL of sample solution and 200 μL of ethanol.  $A$  represents the mixture of 200 μL of ABTS working solution and 200 μL of water.

**2.8.3. OH radical scavenging test.** The hydroxyl radical scavenging activity was evaluated based on the Fenton reaction. Aqueous solutions containing 9 mmol L<sup>-1</sup> ferrous sulfate and 8.8 mmol L<sup>-1</sup> hydrogen peroxide were prepared. Additionally, a solution of 9 mmol L<sup>-1</sup> salicylic acid was prepared in ethanol. The detection principle was based on the generation of hydroxyl radicals through the Fenton reaction, which subsequently react with salicylic acid to form a stable purple product detectable by spectrophotometry.

In this study, a slightly modified procedure based on previous literature<sup>49</sup> was adopted. Specifically, instead of using electron spin resonance (ESR) spectroscopy with DMPO trapping as in the original method, we employed a salicylic acid-based spectrophotometric approach. This modification was made to simplify the experimental process and enhance accessibility, as spectrophotometric methods are more widely available and easier to operate while maintaining sufficient sensitivity for detecting hydroxyl radical scavenging activity.

All mixtures were thoroughly shaken and allowed to stand at 37 °C for 10 minutes in a dark environment. Subsequently, the absorbance was assessed at a wavelength of 530 nm. The rate of OH free radical scavenging was determined utilizing formula (5):

$$\text{Scavenging rate (\%)} = [1 - (B - C)/A] \times 100\%. \quad (5)$$

The revised method remains comparable to the original ESR-based technique in terms of its ability to evaluate anti-

oxidant capacity, and its reliability was confirmed through internal validation and repeatability tests. In the above formula, *B* represents the mixture of 100  $\mu\text{L}$  of hydrogen peroxide solution, 100  $\mu\text{L}$  of sample solution, 100  $\mu\text{L}$  of salicylic acid solution and 100  $\mu\text{L}$  of ferrous sulfate solution. *C* indicates the mixture of 100  $\mu\text{L}$  of hydrogen peroxide solution, 100  $\mu\text{L}$  of sample solution, 100  $\mu\text{L}$  of water and 100  $\mu\text{L}$  of ferrous sulfate solution. *A* represents the mixture of 100  $\mu\text{L}$  of hydrogen peroxide solution, 100  $\mu\text{L}$  of water, 100  $\mu\text{L}$  of salicylic acid solution and 100  $\mu\text{L}$  of ferric sulfate solution.

**2.8.4. Total reducing force test.** The total reducing power was determined using the potassium ferricyanide reduction method. Solutions of 10% potassium ferricyanide, 0.2 mol L<sup>-1</sup> phosphate buffered saline (PBS, pH 6.6), and 1% trichloroacetic acid were prepared. Following a slightly modified procedure based on previous literature,<sup>50</sup> the mixture of sample solution, PBS, and potassium ferricyanide was thoroughly mixed and incubated at 37 °C for 10 minutes in the dark. This modification aimed to stabilize the reaction conditions and minimize oxidative interferences caused by light exposure. After incubation, the mixtures were centrifuged to isolate the supernatant, to which a 0.1% ferric chloride solution was added. The absorbance of the resulting solution was measured at 700 nm. The total reducing force was calculated using formula (6):

$$\text{Total reducing power} = A_1 - A_0. \quad (6)$$

Although the reaction conditions were optimized, the underlying principle remains consistent with ref. 50, and the procedure was internally validated to ensure reproducibility and compatibility with the standard antioxidant assessment. Here, *A*<sub>1</sub> represents the mixture of 1 mL of potassium ferricyanide solution, 1 mL of sample solution, 1 mL of PBS, 1 mL of trichloroacetic acid solution and 1 mL of ferric chloride solution. *A*<sub>0</sub> indicates the mixture of 1 mL of potassium ferricyanide solution, 1 mL of water, 1 mL of PBS, 1 mL of trichloroacetic acid solution and 1 mL of ferric chloride solution.

## 2.9. UHPLC-Q-TOF-MS analysis of the extract

The extract through the UA-MSPD process was conducted using ultra-high performance liquid chromatography quadrupole time-of-flight mass spectrometry (UHPLC-Q-TOF-MS) analysis to identify components that played a role in antioxidant experiments. The specific conditions are discussed below.

Chromatographic system: UHPLC Agilent 1290 (Agilent Technologies, Waldbronn, Germany); mass spectrometry system: Agilent 6520 Q-TOF (Agilent Corporation, Santa Clara, USA); chromatographic column: ACQUITY ZORBAX Eclipse XDB-C18 Column (2.1 × 150 mm, 1.8  $\mu\text{m}$ ); column temperature: 35 °C; flow rate: 0.3 mL min<sup>-1</sup>; mobile phase: 0.1% formic acid solution (A) and acetonitrile (B); the corresponding gradient elution method: 0–30 min, 5–95% (B); injection volume: 2.0  $\mu\text{L}$ .

Electronic spray ionization (ESI): positive and negative ion modes; drying gas (N<sub>2</sub>) temperature: 330 °C; gas flow: 11 L min<sup>-1</sup>; fragmentor voltage: 150 V; nebulizer gas pressure: 35 psig; octopole RF: 750 V; capillary voltage, 4000 V; skimmer

voltage: 65 V; MS scan range: *m/z* 50–1700. In the MS<sup>2</sup> parameters, collision energy (CE) was set as 10 V, 30 V.

## 2.10. Batch experiment

In order to enhance the global applicability of the extraction method, 7 different sources of *Verbena officinalis* L. were used for batch experiments, which were derived from different herbs in different cities in the same province (Puning and Meizhou in Guangdong province), different provinces in the same country (Guangdong, Hebei, Anhui, Shanxi and Yunnan provinces) and different countries (China, Germany and France). Additives in NADES form and non-NADES form were also used to compare the differences in the effectiveness and action of their extracts.

## 2.11. Characterization

Previous research had demonstrated that the extraction efficiency of NPs may be influenced by the physicochemical properties of DESs,<sup>51</sup> such as polarity, viscosity, and pH. Therefore, the properties of eight NADESs were measured (Table S4†) to facilitate the subsequent analysis of their varying extraction efficiencies.

The pH of NADESs was determined utilizing a Mettler-Toledo FE20 pH meter (Shanghai, China) at room temperature. The viscosity of NADESs was measured at 25 °C using an NDJ-9S viscometer (Ningbo, China). Due to the high viscosity of the NADES systems, it was acknowledged that the measurements may be affected by errors of unknown magnitude, which were inherent to the limitations of rotational viscometry in highly viscous media. The polarity of NADESs was assessed employing Nile red dye, an environmentally sensitive fluorescent probe that undergoes a blue shift as the polarity of the solvent increased. The detailed procedure was provided in the ESI.† Nuclear magnetic resonance spectra (<sup>1</sup>H NMR) and Fourier transform infrared (FT-IR) spectra of DES (Bet:Lac = 1:4) and its components were recorded utilizing an AVANCE III-600 MHz spectrometer (Bruker, Germany) and a Nicolet 6700 FT-IR spectrometer (Nicolet, USA), respectively.

To demonstrate the successful preparation of high-purity MOFs, we conducted Scanning Electron Microscopy (SEM) analysis, X-Ray Diffraction (XRD) analysis, X-ray Photoelectron Spectroscopy (XPS) analysis, and Thermogravimetric Analysis (TGA) on these materials. The instruments used were as follows: S-4800 (HITACHI, Japan) for SEM, D8 ADVANCE (Bruker, Germany) for XRD, Thermo Escalab 250Xi (ThermoElectron, USA) for XPS, and STA 449 F5/F3 Jupiter (Netzsch, Germany) for TGA.

## 2.12. Statistical analysis

All data were processed and analysed using GraphPad Prism 9 and SPSS Statistics 27, and then were presented as mean ± standard deviation (SD). One-way analysis of variance (ANOVA) was conducted to evaluate significant differences among multiple groups. Different letters (*e.g.*, *a* > *b* > *c*) were used to indicate significant differences between groups at various levels (*P* < 0.05).

### 2.13. Theoretical computation

All calculations were executed utilizing GaussView 6.0. and Gaussian 16 W. Additionally, Multiwfn 3.8<sup>52</sup> and VMD 1.9.3<sup>53</sup> were employed to analyse the electrostatic potential (ESP)<sup>54</sup> profiles of betaine, lactic acid, and the main targets (hastatoside and cornin). Frontier molecular orbital theory was applied to visualize the lowest unoccupied molecular orbital (LUMO) and the highest occupied molecular orbital (HOMO) of the target molecule before and after adsorption and elution. Electron Localization Function (ELF) analysis was conducted to observe the chemical bond composition of MOF-199. Reduced Density Gradient (RDG), Hirshfeld surface and fingerprint plot analyses were used to investigate weak interactions. Independent Gradient Model based on Hirshfeld partition (IGMH)<sup>55</sup> analysis was carried out on models with intersegment interactions. Gnuplot 5.4 was utilized to illustrate the distribution of specific forces from each RDG and IGMH plot, presented as scatter plots. Detailed calculation parameters and energy calculation formulas are provided in the ESI.†

## 3. Results and discussion

### 3.1. Characterization

In Fig. 2b, the broad absorption peak centered at 3320 cm<sup>-1</sup> is attributed to the characteristic stretching vibrations of the O–H bond. Betaine exhibited characteristic absorption bands at 1625 cm<sup>-1</sup> and 1480 cm<sup>-1</sup>, corresponding to the stretching vibrations of the C=O and C–N bonds, respectively.<sup>56</sup> For lactic acid, the characteristic peak observed at 1702 cm<sup>-1</sup> was associated with the C=O bond. Due to the formation of hydrogen bonds in betaine–lactic acid, the C=O bond of betaine shifted from 1625 cm<sup>-1</sup> to 1720 cm<sup>-1</sup>, while the O–H bond of lactic acid shifted from 3380 cm<sup>-1</sup> to 3360 cm<sup>-1</sup>.<sup>57</sup> To facilitate a clearer comparison, the assignments of the major stretching vibration bands are summarized in Table S5.†

In Fig. 2c, it can be observed that the chemical shift values of hydroxyl hydrogen and carboxyl hydrogen belonging to lactic acid were altered after the formation of DES. For betaine, the chemical shift values of methyl hydrogen and ethyl hydrogen remained largely unchanged after the formation of DES. Furthermore, no new signals were detected in the DES compared to its individual components. These phenomena could be attributed to hydrogen bond formation between betaine and lactic acid.<sup>58</sup> Therefore, the consequence of FT-IR and <sup>1</sup>H NMR collectively confirmed the successful synthesis of DES and the presence of hydrogen bonding.

To further investigate the potential interaction mechanism, SEM was utilized to survey the formation of four MOFs and surface morphology changes of *Verbena officinalis* L. powder before and after treatment with MOF-199. As shown in Fig. 3a–d, the colors of MOF-199, MIL-101(Fe), ZIF-67 and MIL-101(Cr) were blue, brown, purple and green, respectively. SEM revealed that synthetic ZIF-67 exhibited a cubic structure and MOF-199, MIL-101(Cr) and MIL-101(Fe) exhibited a double pyramid octahedral crystal structure. All of them were consistent with pre-

vious studies.<sup>59–62</sup> As shown in Fig. 3e, the surface of the raw powder sample was complete and smooth, and the cell wall structure was complete without obvious rupture. However, after grinding with MOF-199 for a few minutes, the surface of *Verbena officinalis* L. became ruptured, rough, and wrinkled (Fig. 3f). This promoted dissolution of the active ingredients explained why the addition of adsorbents had a higher extraction rate.

As shown in Fig. 3g, the diffraction peaks of MOF-199 were located at the Miller indices (111), (200), (222), (731), and (751), corresponding to the 2θ angles of 6.0607°, 7.499°, 11.662°, 25.678° and 29.673°, respectively. These results were in good agreement with the diffraction patterns reported in the literature [Cambridge Crystallographic Data Centre (CCDC) no. 112954], confirming the successful formation of MOF-199.<sup>63,64</sup> Similarly, the diffraction patterns of ZIF-67, MIL-101 (Fe), and MIL-101 (Cr) matched well with those reported in the literature, verifying their unique crystal structures.<sup>65–67</sup> As shown in Fig. 3h, each spectrum exhibited peaks associated with carbon (C), nitrogen (N), and oxygen (O), which were indicative of the organic linkers present in these MOFs. Additionally, each MOF displayed distinct peaks corresponding to their respective metal ions: copper (Cu) for MOF-199, cobalt (Co) for ZIF-67, iron (Fe) for MIL-101 (Fe) and chromium (Cr) for MIL-101 (Cr). The presence of these characteristic metal ion peaks, alongside the organic framework peaks, served as compelling evidence for the successful synthesis of these MOFs. TGA was a powerful tool for characterizing MOFs as it provided a direct measure of their thermal properties, which were closely related to their structural integrity and composition. As shown in Fig. 3i, all the thermogravimetric curves were consistent with those reported in the literature, which proved the high purity of the four MOFs.<sup>68–71</sup> Therefore, all the above characterization results together confirmed the successful synthesis of MOF materials.

### 3.2. Single factor optimization process

**3.2.1. Type of adsorbent.** Three commercial adsorbents, C18, COOH, and PWCX, were used in this experiment to compare their extraction efficiencies with those synthetic MOF materials. C18, or octadecyl silica gel, was a solid phase extraction adsorbent based on silica gel modified with octadecyl, noted for its ease of operation, versatility, and reusability. As for COOH, the carboxyl group within its carboxyl functional group possessed strong hydrophilic and electrophilic properties, which enabled it to interact with the adsorbent through hydrogen bonding, van der Waals forces, electrostatic attraction, and so forth, thereby achieving the effect of adsorption and separation. Regarding PWCX, a mixed adsorbent, it not only possessed non-polar hydrophobic properties but also had a weak cation exchange function, belonging to the category of polymer matrix weak cation exchange solid phase extraction adsorbents. As shown in Fig. 4c, MOF-199 exhibited the best extraction performance, surpassing the three commercial adsorbents as well as the other three MOFs. This superior performance can be attributed to the unique porous structure and large surface area of MOF-199, which increased its interaction sites with the target compounds, significantly enhancing its adsorption capacity.<sup>72</sup>

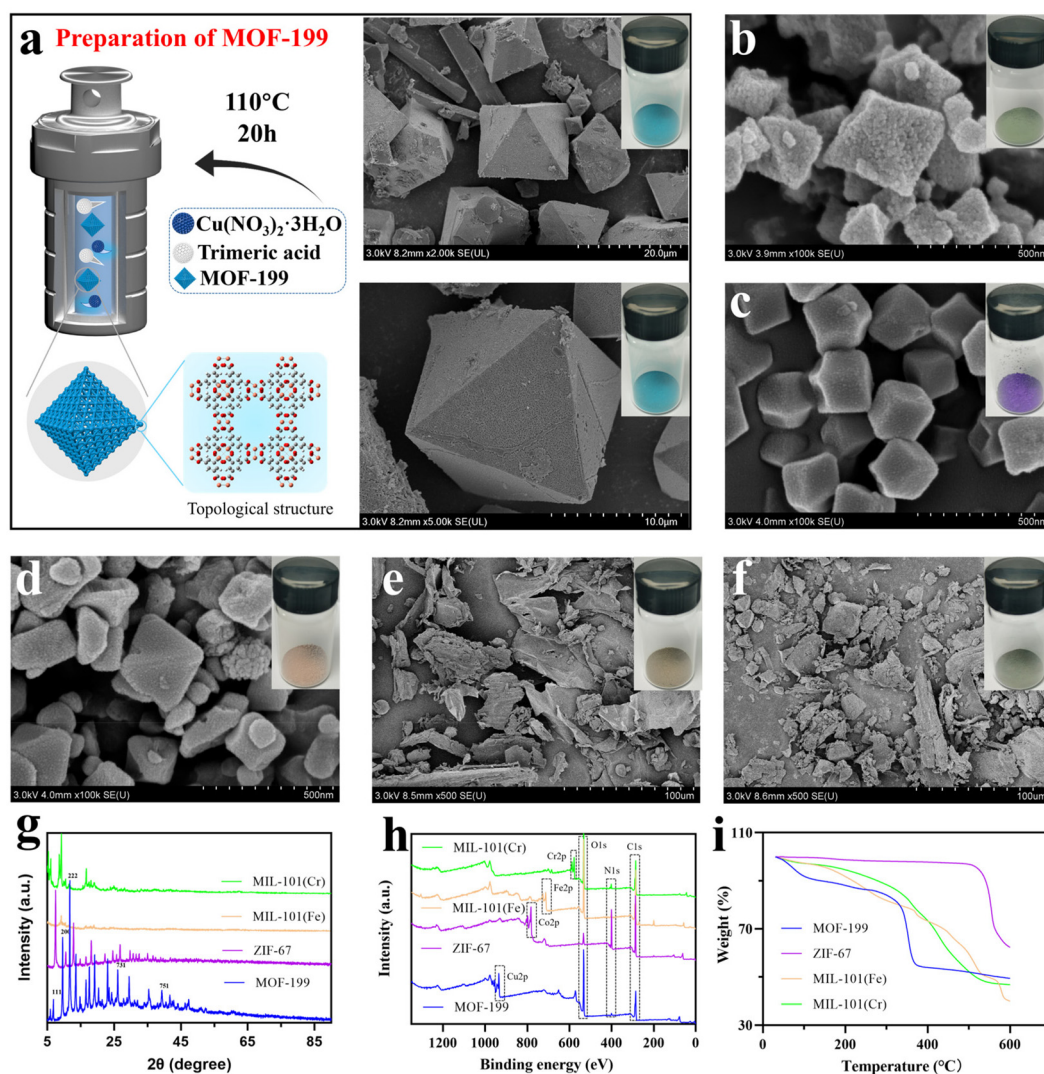


**Fig. 3** (a) SEM image of MOF-199. (b) SEM image of MIL-101(Cr). (c) SEM image of ZIF-67. (d) SEM image of MIL-101(Fe). (e) SEM image of *Verbena officinalis* L. powder. (f) SEM image of the ground mixture of MOF-199 and *Verbena officinalis* L. powder. (g) XRD curves of MOFs. (h) XPS curves of MOFs. (i) TGA curves of MOFs.

However, the specific surface area of C18, COOH, and PWCX was low, and their pore structure was not as regular as that of MOF-199, which limited their adsorption capacity.<sup>73–75</sup> Similarly, the poor adsorption efficiency of the other three MOFs may be due to their lack of strong coordination metal sites like MOF-199.<sup>76–78</sup> Therefore, to determine the optimal extraction conditions, MOF-199 was used as the preferred adsorbent for optimizing the next set of extraction factors.

**3.2.2. Sample to adsorbent ratio.** As shown in Fig. 4d, the extraction capacity for the 2:1, 1:1, and 1:2 ratios of the medicinal material to the adsorbent was higher compared to the 1:0 ratio. This indicated that the addition of MOF-199 can enhance the extraction efficiency of *Verbena officinalis* L. When the amount of adsorbent was gradually increased (10 mg, 20 mg and 40 mg), the extraction efficiency first increased and then decreased. This phenomenon can be explained by the structural characteristics of MOF-199. An appropriate amount

of MOF-199 improved adsorption capacity by facilitating interactions with the target compound, allowing more of the target to be eluted. However, excessive amounts of the adsorbent may lead to an envelope effect, wherein the target substance is overly enclosed, reducing the efficiency of elution and making it more difficult to recover the target compound.<sup>79</sup> Therefore, to determine the optimal extraction conditions, the 2:1 sample to adsorbent ratio will be used as the ideal dosage for further optimization of extraction parameters.

**3.2.3. Grinding time.** As shown in Fig. 4e, the extraction capacity of *Verbena officinalis* L. initially increased and then decreased with the gradual increase in grinding time. This can be attributed to the fact that moderate grinding time and intensity effectively disrupted the physical structure of the medicinal powder, enhancing the interaction between the adsorbent and the target components, which improved the extraction efficiency. However, excessive grinding time can

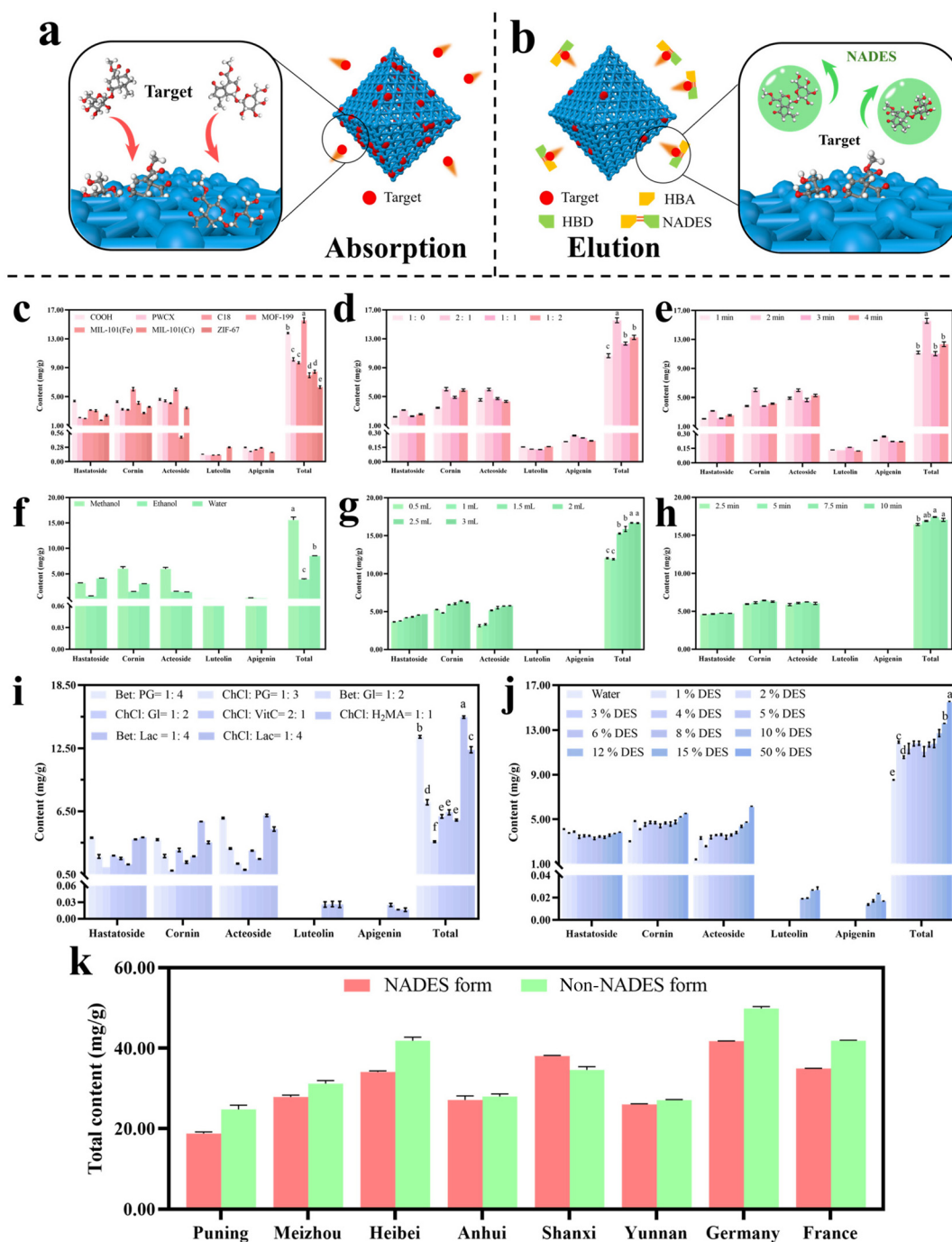


**Fig. 4** (a and b) Schematic diagram of MSPD adsorption and the elution process. Single factor optimization results: (c) type of adsorbent, (d) sample to adsorbent ratio, (e) grinding time, (f) type of traditional eluent, (g) extractant volume, (h) extraction time, (i) type of the DES eluent and (j) DES dosage. Different letters imply significant differences at different levels. (k) Batch tests from different sources. The error bar represents RSD ( $n = 3$ ).

lead to overly mighty adsorption of the target components by MOF-199. This, in turn, hindered the elution process, making it difficult to recover the target substance. Therefore, to identify the optimal extraction conditions, a grinding time of 2 minutes will be used as the ideal parameter for further optimization of extraction factors.

**3.2.4. Type of eluent.** To solve the problem of slow mass transfer caused by the high viscosity of DESs, all DES samples

were diluted with equal volumes of water to eliminate individual differences. As shown in Fig. 4f and i, the extraction efficiency of eight DESs was compared. Among them, Bet:Lac = 1:4 exhibited the best extraction efficiency in DESs. The extraction capacity of Bet:PG = 1:4 and ChCl:Lac = 1:4 was slightly lower than Bet:Lac = 1:4 but still higher than the water. The extraction efficiency of ChCl:PG = 1:3, ChCl:Gl = 1:2, ChCl:Vit C = 2:1, and ChCl:H<sub>2</sub>MA = 1:1 was lower than

water but surpassed that of ethanol. An interesting observation was that luteolin and apigenin were only extracted by organic reagents and acid-based DESs, likely due to their strong acidity. Additionally, DESs based on lactic acid and propylene glycol achieved the highest yields, particularly for hastatoside and acteoside.

These findings highlighted the unique properties of DESs, which provided advantages over traditional solvents in most cases. The differing extraction capacities among DESs can be attributed to the varying types of HBD and HBA. This affected the physicochemical properties of DESs, such as the strength of hydrogen bonds, viscosity, and pH levels, among others, which were also directly linked to the extraction efficiency of DESs. Gygli *et al.*<sup>80</sup> found that whether the viscosity of DESs was too high or too low will affect its performance. Low viscosity indicated that the hydrogen bond system was not perfect, which was not conducive to the extraction function. However, too high viscosity will affect the conduction of extracted components, and thus also reduce the extraction effect. So, the superior extraction efficiency of Bet:Lac = 1:4 may be due to its moderate acidity and appropriate viscosity.

For traditional solvents, the extraction amount of methanol was higher than that of ethanol and water, mainly concentrated in cornin and acteoside. Although water extraction yielded minimal amounts of the five ingredients, this does not necessarily mean that the antioxidant capacity of the water extract is weaker than that of the organic solvent extract. As a polar solvent, water can often extract more polar antioxidant components. Moreover, its environmentally friendly nature and the absence of recycling requirements make it an ideal partner for NADES as a green solvent.<sup>81</sup> Combined with the best DES (Bet:Lac = 1:4), we hypothesized that the combination of the two could make the antioxidant effect of the extract better, taking advantage of the greenness of water and the high extraction of DESs.

At the same time, it was pivotal to find the most economical point to reduce the amount of DESs as much as possible while ensuring the high extraction rate, which can not only avoid the recovery of DESs, but also maximize the antioxidant capacity of the extract. This was attributed to the fact that the DES we use comes from natural ingredients, making it free from recycling in the extraction field.<sup>82</sup> However, since the cost of NADES is generally higher than non-NADES, it would be better to use a small amount of NADES to achieve a higher extraction rate. So, to further investigate the impact of concentration of DESs on extraction capacity, subsequent studies were conducted using water containing varying concentrations of DES (Bet:Lac = 1:4).

**3.2.5. DES dosage.** As shown in Fig. 4j, the total extraction yields gradually increased with the rising proportion of DESs in water. Notably, when the concentration of DESs reached 10%, it facilitated the water-based extraction of luteolin and apigenin, demonstrating that the addition of DESs enhanced the extraction capacity of water. The extraction rate of 1% DESs was observed to be higher than that of 2% DES but lower than

3% DES, suggesting the existence of at least one maximum value within the range from pure water to 2%. And this maximum value was the most economic point needed to find in the RSM experiment subsequently. Considering both economy and efficiency, water containing 1% DES was selected as the optimal eluent for subsequent optimization.

**3.2.6. Extractant volume.** Extractant volume was an important parameter for evaluating whether the target compounds can be completely eluted from the adsorbent. As shown in Fig. 4g, the extraction capacity of *Verbena officinalis* L. increased initially with the gradual increase of extractant volume and then reached saturation. This phenomenon increased due to an insufficient extractant volume, which prevented complete extraction of the target compounds, resulting in some remaining undissolved in DESs. Therefore, to determine the optimal extraction conditions, 2.5 mL was selected as the ideal extractant volume for further optimization of extraction factors.

**3.2.7. Extraction time.** The UA-MSPD technique could enhance the extraction process by applying ultrasonic waves. Among the factors influencing UA-MSPD, extraction time also played a crucial role. As shown in Fig. 4h, the extraction capacity of *Verbena officinalis* L. increased initially with the extension of extraction time but then began to decrease. This was because a longer ultrasound time had allowed the target compounds to dissolve more thoroughly in DESs. However, excessive extraction time can result in the decomposition of certain active components in *Verbena officinalis* L. or trigger chemical reactions, thereby reducing the extraction efficiency. Consequently, 7.5 minutes was selected as the optimal extraction time for UA-MSPD of *Verbena officinalis* L.

### 3.3. RSM optimization process

The single-factor optimization experiments revealed a significant impact of five quantitative parameters on the extraction process of *Verbena officinalis* L. and their optimal ranges were adsorbent dosage (0–20 mg), grinding time (1–3 min), DES dosage (0–2%), extractant volume (2–3 mL), and extraction time (5–10 min), respectively. To further investigate the key parameters influencing the extraction efficiency, the Box-Behnken design was employed to design the experimental scheme. Expert Software (version 13) was used to facilitate the establishment of the model to clarify the relationship between DES dosage with other four extraction parameters. The experimental response variable was described by using the following formula:

$$Y = 20.01 - 0.8112A + 0.0191B + 3.04C + 0.1788D + 0.3038E - 0.4494AB - 0.3332AC - 0.6621AD - 0.212AE + 0.0018BC - 0.4858BD - 0.9278BE - 0.1638CD + 0.1709CE + 0.2938DE - 0.1476A^2 - 0.0222B^2 - 3.24C^2 + 0.0941D^2 + 0.5822E^2$$

In this context, *Y* represents the overall extraction yield of the targeted components, whereas *A*, *B*, *C*, *D*, and *E* correspond

to the adsorbent dosage, grinding time, DES dosage, extractant volume, and extraction time, respectively. The ANOVA underscored the dependability and precision of the model fitting, as evidenced in Table S6.† Notably, the “*P*-value” was below 0.0001, demonstrating significant fitting accuracy. Additionally, the “Lack of Fit” ( $P = 0.1711$ ) and the correlation coefficient  $R^2$  (0.9920) had substantiated the establishment of a robust and credible regression model within the study conducted. The adjusted  $R^2$  (0.9856) and predicted  $R^2$  (0.9700), differing by less than 0.2, had suggested a strong alignment between the predicted and experimental values, emphasizing the model's exceptional regression capabilities in the past tests. The coefficient of variation ( $CV = 1.60\%$ ,  $<10\%$ ) had further reinforced the high reliability and accuracy of the experiments conducted. In conclusion, this model had offered accurate and reliable predictions for the extraction yield of target substances in *Verbena officinalis* L.

The order of influence of each extraction parameter on the total extraction rate was as follows:  $A-A = C-C > E-E > D-D > B-B$ . The interaction terms ( $AB$ ,  $AD$ ,  $BD$ ,  $BE$ , and  $DE$ ) and the quadratic terms ( $C^2$  and  $E^2$ ) were significant, showing that the five factors were interrelated and influenced each other on the total extraction yield of analytes.

It can be observed from Fig. 5a that when the interrelated influence of the other four factors with DES dosage was investigated, the extraction yield of *Verbena officinalis* L. consistently increased with the rising concentration of DESs, peaking at approximately 1.5%. However, the extraction yield decreased when concentration of DESs exceeded 1.5%, which aligned with the results of single-factor optimization, indicating that there was an extreme point near 1.5% DES. Additionally, the graphical comparison of the predicted and actual extraction yields demonstrated that the mathematically calculated values closely match the experimental values. The normal probability plot of residuals (% normal probability compared to the internally studied residuals) showed no significant deviation from normality, indicating the robustness of the model.<sup>35</sup>

Therefore, based on the analysis of the model and the response surface, the optimal extraction conditions were determined as follows: the adsorbent dosage was 14.22 mg, grinding time was 1.18 min, DES dosage was 1.52%, extractant volume was 2.92 mL, and extraction time was 9.57 min. To verify the extraction performance of this model, 20 mg of *Verbena officinalis* L. was extracted under these optimal conditions in triplicate. The results indicated that the extraction rate of five target compounds was  $22.99 \pm 0.67 \text{ mg g}^{-1}$ , with minimal deviation from the predicted value of  $22.13 \text{ mg g}^{-1}$ . These findings confirmed the accuracy of response surface optimization in reliably predicting the extraction yield and the impact of extraction parameters.

### 3.4. Analysis of the machine learning results

**3.4.1. Performance evaluation of machine learning models.** This study undertook the development and evaluation of six distinct ML models aimed at predicting the extraction yield of *Verbena officinalis* L. As shown in Fig. 5c, since the Train

$R^2$  and Test  $R^2$  values were close, all models were not overfitted. CatBoost achieved the highest Train  $R^2$  and Test  $R^2$  values, with the lowest RMSE, delivering the best performance. Compared to other Boosting Tree models, it outperformed mainly due to its native support for categorical features, the ordered encoding method that prevented target leakage, symmetric tree structure, efficient default parameters, and GPU acceleration. These features enhanced the model's generalization ability, training efficiency, and robustness to noisy data, particularly in scenarios with abundant categorical features or complex data distributions. So CatBoost was selected for subsequent research.

**3.4.2. Model interpretation.** To gain deeper insight into the effect of various attributes in the extraction yield of *Verbena officinalis* L., feature importance and SHAP value analysis was conducted (Fig. 5d and e). The higher the value of importance, the greater the degree of influence of the factors, so DES dosage was the most important factor in the extraction process. Additionally, the SHAP value less than 0 indicated that the feature variable had a negative impact on the target variable, and a SHAP value greater than 0 indicated that the feature variable had a positive impact on the target variable. Therefore, the greater the dosage of DES had a positive effect on the extraction yield rather than a negative effect, which was consistent with the results shown in Fig. 4j. Meanwhile, the adsorbent dosage and grinding time also had a positive impact on the target variable, indicating the effect of MOF's interaction. These findings underscored the critical roles these parameters play in optimizing the efficiency of the UA-MSPD process, providing a clearer understanding of how adjustments to these variables can enhance the extraction yield of target components. Among them, the DES dosage was the most critical influence, which once again proved that a small amount of this green substance can greatly increase the extraction amount of *Verbena officinalis* L. Therefore, in the follow-up antioxidant experiment, an aqueous solution containing 1.52% NADES was used to extract *Verbena officinalis* L. and compare the antioxidant capacity of the extract with that of traditional ethanol extraction.

**3.4.3. GUI model.** To support the development of the CatBoost model, we packaged the files [“catboost\_optimized.pkl” and “scaler.pkl”] and developed a Graphical User Interface (GUI) model (Fig. S2†) in Python 3.13.1 for the use by future researchers. This model allowed users to quantitatively predict the extraction yield of *Verbena officinalis* L. by inputting values of five influencing factors, thereby facilitating the optimization of experimental design and practical deployment. The relevant source code of GUI was provided in the ESI.† Users can simply open the file named “GUI.python file” to start using the model. Other codes about model's training, feature importance analysis and SHAP analysis are available online at <https://github.com/17609858895/EDS>. The complete machine learning process is shown in Fig. 5b.

### 3.5. Method validation

As shown in Table S7,† the five target compounds demonstrated a strong linear relationship within the configured gra-

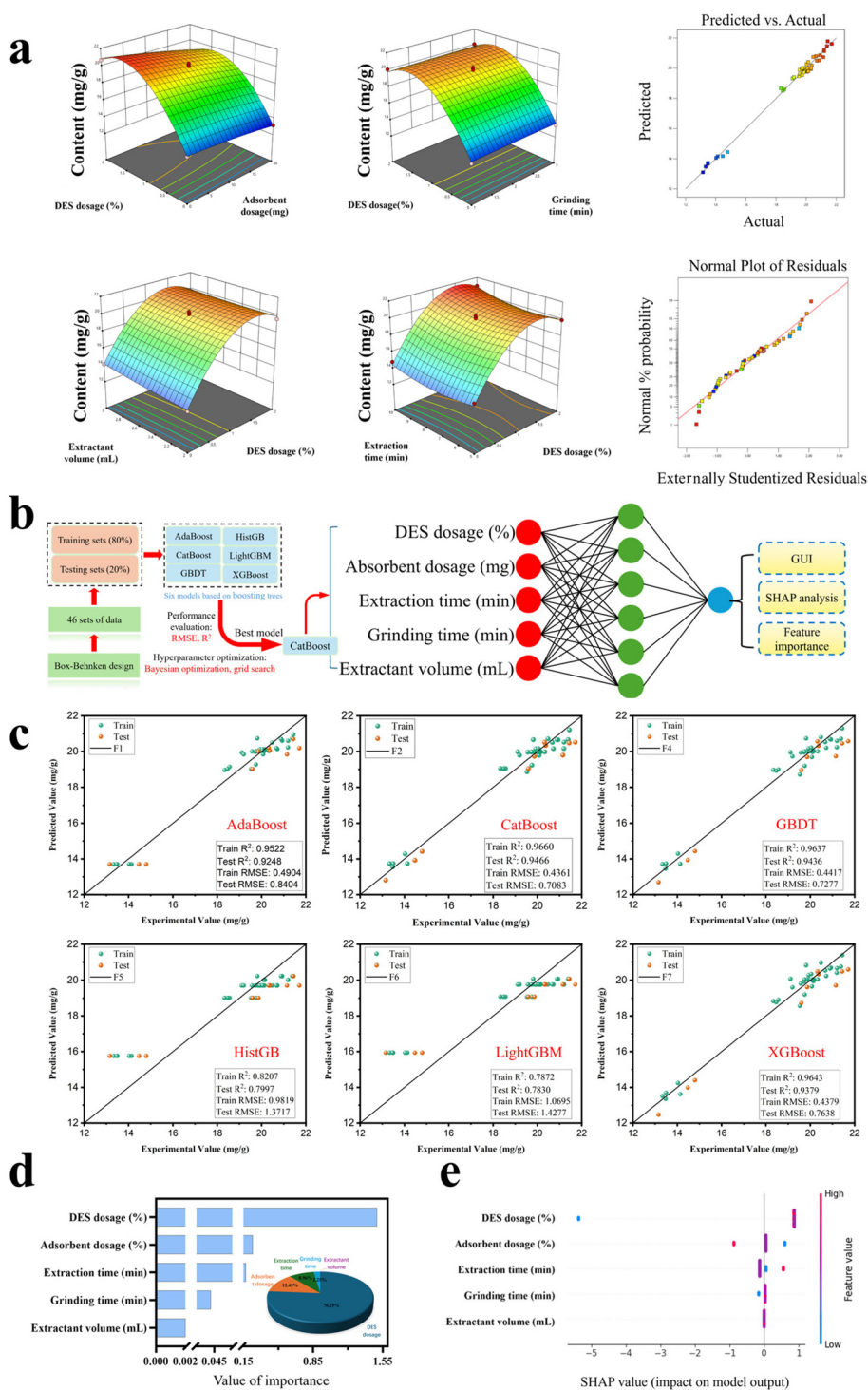


**Fig. 5** (a) Scatter plot and data distribution of the experimental and predicted values. (b) Three-dimensional response surface of DES dosage with other factors, plot of the predicted values *versus* the experimental values, the normal % probability residuals and the studentized residuals. (c) Machine learning flowchart. (d) Feature importance analysis. (e) SHAP value visualization.

cient concentration range ( $R^2 > 0.99$ ), confirming that the regression curve equation can accurately quantify each target compound. The low limits of detection (0.088–0.600  $\mu\text{g mL}^{-1}$ ) and limits of quantification (0.292–2.000  $\mu\text{g mL}^{-1}$ ) indicated that each target compound can be easily detected and quanti-

fied at low concentrations. From Table S8,<sup>†</sup> it was evident that the relative standard deviation (RSD) for repeatability of the five target compounds was below 2.75%, indicating good repeatability of the HPLC method for the same sample. Additionally, the precision RSD was below 2.99%, and the

stability RSD was below 2.93%, demonstrating the high stability of the HPLC method and the standard solvent used. As indicated in Table S9,† the recoveries of the five target compounds varied between 98.80% and 108.54%, with all RSD values remaining below 2.33%. These results confirmed that the method used in this experiment was both reliable and accurate.

### 3.6. Analysis of the antioxidant capacity of the extract

To detect the antioxidant ability of the extract from UA-MSPD and ethanol, a series of antioxidant experiments were carried out, including assessments of DPPH, ABTS, and OH radical scavenging abilities, as well as the total reducing power. Meanwhile, the Vit C solution acted as a positive control.

The DPPH free radical scavenging capacity of the extracts is illustrated in Fig. 6a. An increase in the concentration of both extracts corresponded with an enhancement in their DPPH free radical scavenging efficiency. Notably, at equivalent concentrations, the UA-MSPD extract exhibited a significantly greater scavenging rate compared to the ethanol extract, suggesting that the UA-MSPD method effectively extracted a higher quantity of antioxidant components from *Verbena officinalis* L. The IC<sub>50</sub> values for the UA-MSPD extract and the ethanol extract were determined to be 1.77 mg mL<sup>-1</sup> and 15.85 mg mL<sup>-1</sup>, respectively.

The ABTS free radical scavenging abilities of the two extracts at varying concentrations are presented in Fig. 6b. At comparable concentrations, the UA-MSPD extract demonstrated a superior scavenging rate relative to the ethanol extract, although both extracts exhibited a lower activity than Vit C. The IC<sub>50</sub> values for the UA-MSPD extract and the ethanol extract were found to be 2.83 mg mL<sup>-1</sup> and 26.33 mg mL<sup>-1</sup>, respectively.

The OH free radical scavenging capacity of the extracts was assessed using the Fenton reaction, as depicted in Fig. 6c. The scavenging rates for the UA-MSPD extract, ethanol extract, and Vit C all increased with concentration. At the same concentration, the OH radical scavenging rate of the UA-MSPD extract surpassed that of the ethanol extract, although both were inferior to that of Vit C. The IC<sub>50</sub> values for the UA-MSPD extract and the ethanol extract were recorded at 0.16 mg mL<sup>-1</sup> and 1.11 mg mL<sup>-1</sup>, respectively, indicating that both extracts exhibited a significant scavenging effect on OH radicals, with the UA-MSPD extract demonstrating superior efficacy compared to the traditional ethanol extract.

The results of the total reducing power test are illustrated in Fig. 6d. The reducing power of all samples increased with concentration. While the reducing capacities of the two extracts were significantly lower than that of Vit C at equivalent concentrations, the UA-MSPD extract consistently demonstrated a greater reducing power compared to the ethanol extract.

The above results collectively demonstrated that the UA-MSPD extract significantly enhanced the ability to scavenge DPPH, ABTS, and OH free radicals, as well as improved the reducing power, compared to the traditional ethanol extraction method. This confirmed that a small amount of DES added to

water to extract the active ingredient of *Verbena officinalis* L. can have a stronger antioxidant capacity than ethanol extraction, so the green and high efficiency of this technology can be achieved.

### 3.7. Extract composition analysis

The UA-MSPD extract was analyzed by UHPLC-Q-TOF-MS to determine its main antioxidant components. By analyzing the primary and secondary mass spectra of positive and negative ion patterns, and cross-comparing with databases and the existing literature, 10 active components were identified. Details of the specific components are shown in Table S10.†

The ingredients include 3 flavonoids (luteolin, apigenin and quercetin), 3 iridoids (hastatoside, cornin and rehmannitin) and 4 phenylethanol glycosides (acteoside, cistanoside F, cistanoside C and 2'-acetylverbascoside). Phenylethanol glycosides were the main active ingredients of that extract. This comprehensive analysis provided important insights for further exploration of the antioxidant properties of *Verbena officinalis* L.

### 3.8. Batch experiment results

In order to explore the suitability of the method for *Verbena officinalis* L. of different origins and whether the hydrogen bond system of NADES in water will be broken at trace concentrations, DES form and non-DES form eluents will be used to compare the extraction yield and antioxidant capacity of various *Verbena officinalis* L. As shown in Fig. 4k, there are differences in the extraction yield of different solvents for the herbs from different places. In addition to the *Verbena officinalis* L. derived from Shanxi, the non-DES form had a higher extraction amount for the herbs. However, when we compared water, 1.5% DES water and 1.5% non-DES water as eluents, we found that the antioxidant capacity of the solvent in the form of DES was stronger than the other two, as shown in Fig. 6f. From this, we can conclude that although the extraction yield of DES in a specific target was not as good as that of non-DES, its residual hydrogen bond system can protect the active site of antioxidant components and improve its effect.

As illustrated in Fig. 6g, the antioxidant experimental results of 7 kinds of *Verbena officinalis* L. showed that the MSPD extract had a stronger antioxidant capacity than the ethanol extract, which confirmed the universality of this extraction method in different cities, different provinces and different countries.

### 3.9. Calculation results

To investigate the role of NADES in the extraction process, the optimal configuration of DES (Bet : Lac = 1 : 4) was used as a representative to simulate its binding with the target components. For hastatoside and cornin, which were the most abundant in the extract, were also used as the representatives of the simulated targets.

**3.9.1. DES composition analysis.** As shown in Fig. 2d, three different configurations of DESs (DES-1, DES-2 and DES-3) were constructed. Based on the results of the energy calcu-

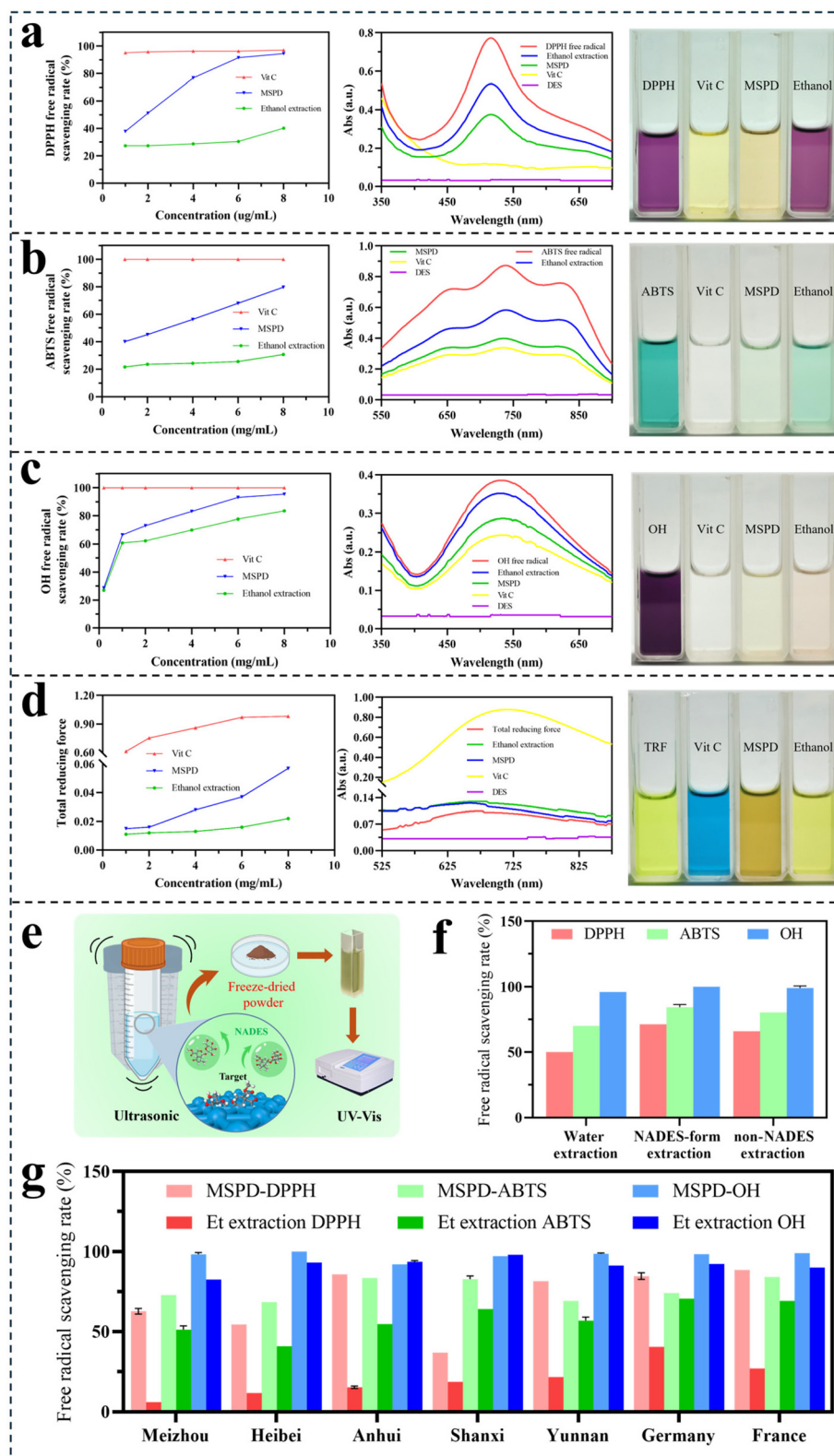


**Fig. 6** (a) DPPH free radical scavenging test. (b) ABTS free radical scavenging test. (c) OH free radical scavenging test. (d) Total reducing force (TRF) test. (e) Schematic diagram of the antioxidant test. (f) The antioxidant test of NADES formation or not. (g) Batch antioxidant tests from different sources. The error bar represents RSD ( $n = 3$ ).

lations, the  $\Delta G_{\text{int}}$  of DES-3 was  $-109.30 \text{ kcal mol}^{-1}$ , which was lower than  $-104.34 \text{ kcal mol}^{-1}$  of DES-2 and  $-92.38 \text{ kcal mol}^{-1}$  of DES-1.  $\Delta G_{\text{int}}$  indicated the interaction strength and stability of the system. A smaller  $\Delta G_{\text{int}}$  indicates that the internal DES force is stronger, and the structure of this DES is more stable, which was more likely to be the true conformation from the microscopic perspective.<sup>83</sup> Therefore, DES-3 was regarded as the optimal configuration for subsequent simulations.

**3.9.2. ESP analysis.** ESP is a method used to observe the electrostatic characteristics of an uncertain charge distribution region. The blue dots (related to nucleophilicity) and red dots (related to electrophilicity) represented the negative extremal points and positive extremal points of the ESP, respectively.<sup>84</sup> As shown in Fig. 2e, the extreme points of negative charge of betaine were mainly distributed around carbonyl oxygen, while the extreme points of positive charge were mostly positioned nearby quaternary ammonia. The negative charge extreme points of lactic acid were mainly distributed around carbonyl oxygen and hydroxyl oxygen, while the positive charge extreme points were mostly positioned nearby hydroxyl hydrogen. ESP of DES exhibited an interaction between the hydroxyl hydrogen of lactic acid and the carbonyl oxygen of betaine, which was attributed to the hydrogen bond connection between the hydrogen bond donor and the hydrogen bond acceptor. These results indicated the existence of a hydrogen bond inside the DES.

As shown in Fig. 7b and c, the hydrogen bond donor sites of hastatoside and cornin were primarily distributed on the hydroxyl hydrogen of the tetrahydropyran ring, while the hydrogen bond acceptor sites were mainly found on the hydroxyl oxygen of the tetrahydropyran ring and the carbonyl group of the monoterpene ring. These regions may be one of the hydrogen bond sites where the DES exerted its protective effect. According to Fig. 7a, for MOF-199, the negative charge extreme points were concentrated near oxygen atoms, while the positive charge extreme points were located near copper atoms, reflecting the significant electronegativity difference between these atoms.

According to Table S11,<sup>†</sup> the positive surface area of the molecular surfaces of betaine, lactic acid, hastatoside, cornin, and MOF-199 exceeded the negative surface area. Additionally, the molecular polarity index (MPI) of hastatoside was higher than that of cornin, suggesting that electrostatic interactions play a more significant role in its interaction.<sup>85</sup> Furthermore, the polarity of lactic acid closely matched that of hastatoside and cornin, which may explain why a lactic acid-based DES achieved the highest extraction yield.

**3.9.3. Interaction force analysis.** Fig. 7d presents the ELF topography map and projection map of MOF-199. In this figure, the blue regions indicated the areas of electron accumulation, while the red regions indicated electron depletion. It was evident that the orbital overlap and electron localization between copper (Cu) and oxygen (O) atoms were weaker than that for any other atomic combination, suggesting that Cu and O were coordinated rather than forming a covalent bond.

Fig. 7e and f show the weak interactions between MOF-199 and the target compounds. The mapping function used was

$d_{\text{norm}}$ , with a color scheme of blue–white–red. The red regions represent smaller  $d_{\text{norm}}$  values, indicating close intermolecular contact and strong interactions, while the white regions indicate weaker van der Waals interactions compared to hydrogen bonds. In the fingerprint plots, peaks in the lower-left corner reflect the central fragment (MOF-199) as the hydrogen bond donors ( $d_i > d_e$ ) and the hydrogen bond acceptors ( $d_i < d_e$ ) interacting with the guest molecules (hastatoside and cornin).

The analysis showed that MOF-199–cornin interactions exhibited a hydrogen bond acceptor peak, while MOF-199–hastatoside interactions exhibited both a hydrogen bond acceptor peak and a hydrogen bond donor peak. Notably, the hydrogen bond donor peak in hastatoside was atypical, representing a coordination force between the lone pair electrons of the oxygen atom in hastatoside and the empty orbital of the copper atom in MOF-199. Therefore, MOFs can adsorb target materials through a variety of interaction forces, thereby enhancing their extraction amount.

Different colors of RDG and IGMH represented distinct weak interaction forces: the blue areas indicate hydrogen bonding, the green areas correspond to van der Waals forces, and the red areas indicate repulsive forces. Fig. 7g illustrates the distribution of weak interaction forces within the DES molecules. It was observed that van der Waals forces and repulsive forces were mainly present within individual molecules of betaine and lactic acid, whereas the interaction between betaine and lactic acid was predominantly driven by hydrogen bonds, confirming that DES was synthesized through hydrogen bonding. This finding aligned with the outcomes of the ESP analysis.

Fig. 7h and i depict the weak interaction between DES and the two target compounds. Van der Waals forces were dominant in the interaction between the two objects, but hydrogen bonding forces existed in both. He *et al.*<sup>86</sup> proposed that the hydrogen bonding effect of DES could effectively protect the target components to avoid its inactivation before it plays its role. This special protective effect may be the reason why DES can enhance the antioxidant capacity of the extract.

**3.9.4. Frontier molecular orbital analysis.** Fig. 8c and d show the HOMO/LUMO distribution and the variation in the energy gap ( $E_{\text{gap}}$ ) of *Verbena officinalis* L. during the MSPD process. Prior to the process, the HOMO and LUMO of hastatoside and cornin were localized within their monoterpene rings. After elution with DES, the HOMO and LUMO of hastatoside and the HOMO of cornin remained in the monoterpene rings, while the LUMO of cornin shifted to the DES. For systems involving MOF-199, the HOMO and LUMO were consistently retained on the coordination bonds within the MOF, as shown in Fig. 8a.

$E_{\text{gap}}$ , defined as the difference between LUMO and HOMO energy levels, was a key factor in determining the stability and reactivity of a system. A smaller  $E_{\text{gap}}$  indicated better stability and higher reactivity.<sup>87</sup> Before the extraction process, the  $E_{\text{gap}}$  values for hastatoside and cornin were 5.29 eV and 5.50 eV, respectively. Following adsorption and elution, the  $E_{\text{gap}}$  values decreased to 3.44 eV and 5.24 eV for hastatoside, and 1.88 eV

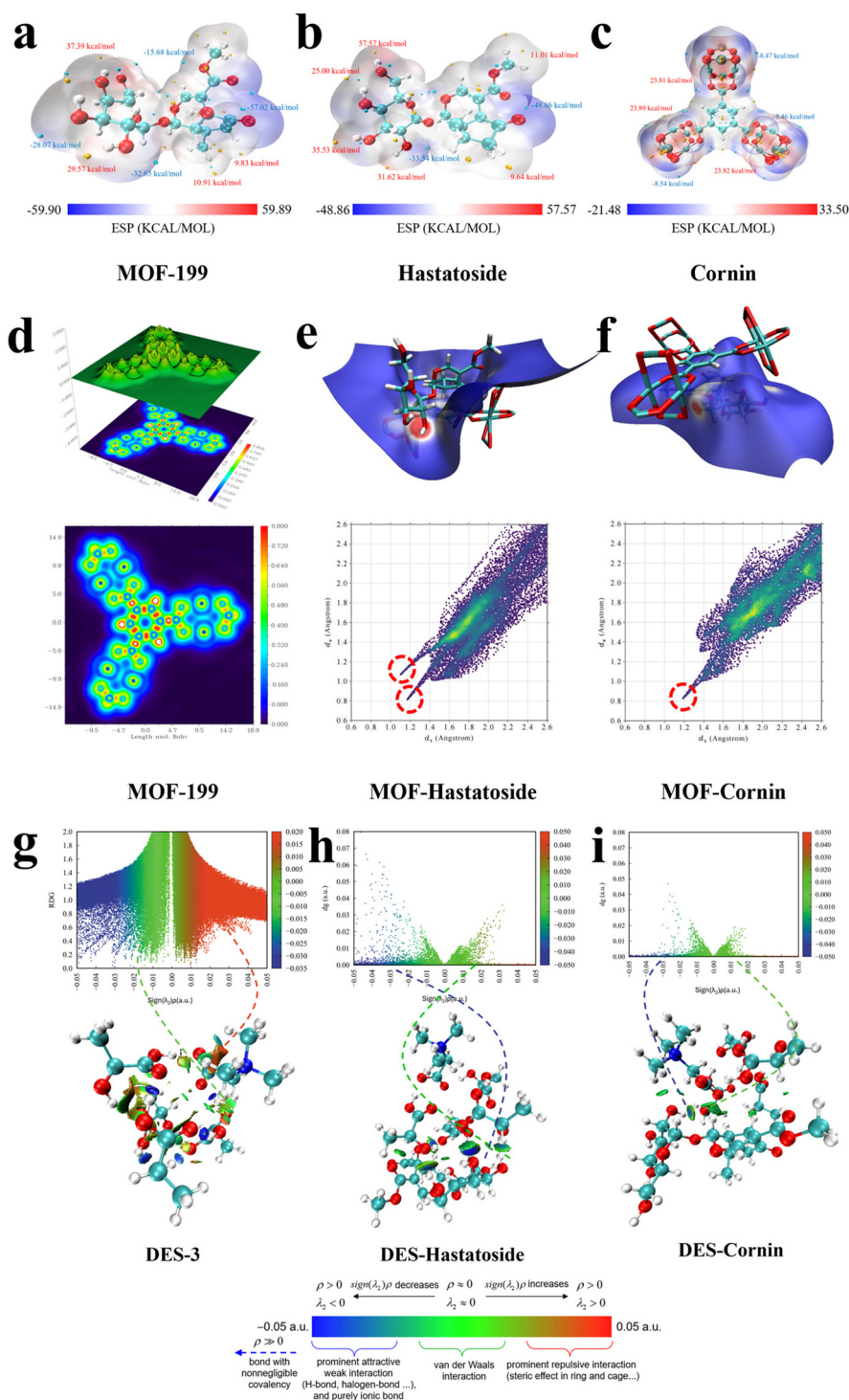


**Fig. 7** (a–c) ESP distribution of MOF-199, hastatoside and cornin. (d) ELF topography and the projection map of MOF-199. (e and f) Colored maps of  $d_{\text{norm}}$  on the Hirshfeld surface and the corresponding fingerprint plot of MOF-targets. (g)  $\text{Sign}(\lambda^2)\rho$  colored RDG scatter plot and colored function  $\delta g^{\text{inter}}$  map of the best conformation of DES (isosurface value = 0.05 a.u.). (h and i)  $\text{Sign}(\lambda^2)\rho$  colored IGMH scatter plot and colored function  $\delta g^{\text{inter}}$  map of DES targets (isosurface value = 0.05 a.u.).

and 5.10 eV for cornin, respectively. This suggested that both the adsorption process by MOF and the elution process by DES were facile to implement, thereby reducing the system energy of the complex system. This analysis elucidated, from a micro-

scopic perspective, the reasons behind the enhanced adsorption efficiency of MOF and the protective role of DES, which collectively contributed to the increased extraction yield and improved antioxidant capacity of the active components.

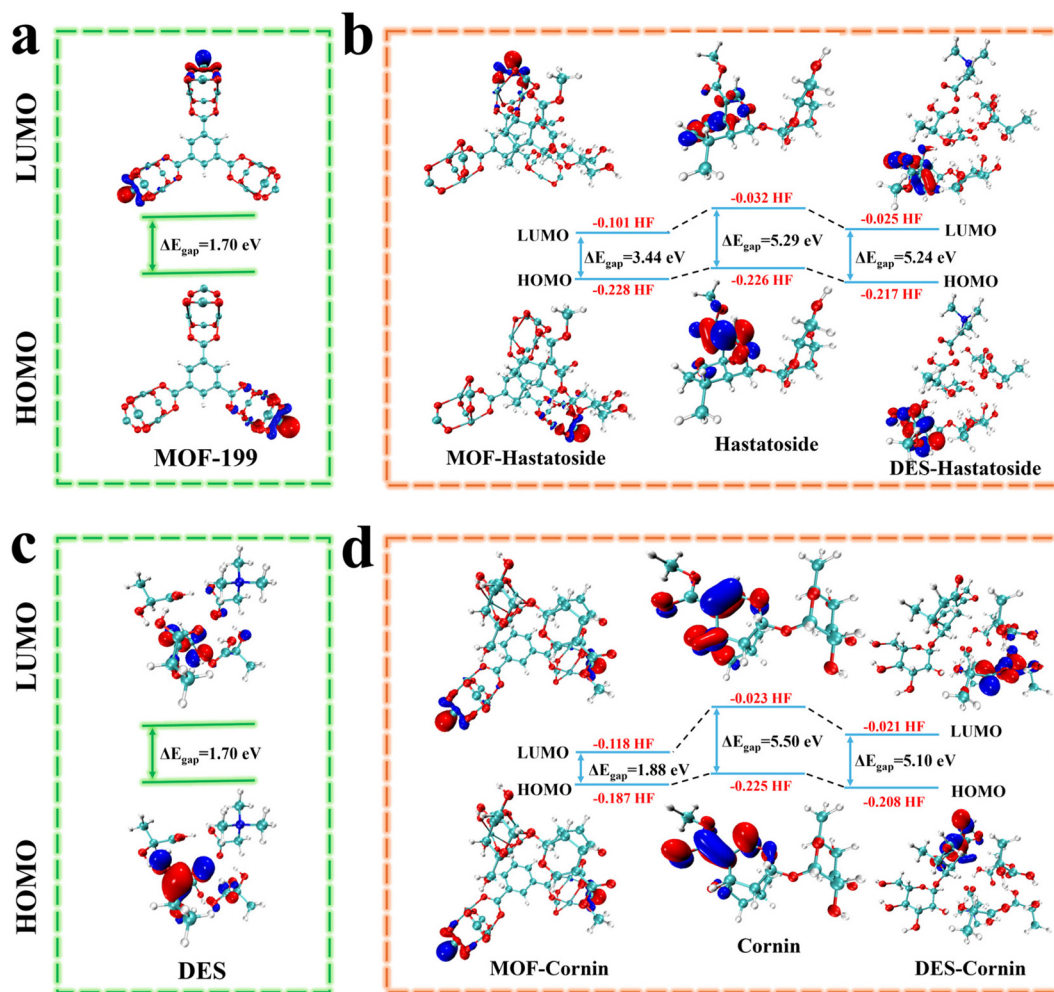


Fig. 8 (a) The HOMO and LUMO of MOF-199. (b) The HOMO and LUMO of hastatoside before and after adsorption or elution. (c) The HOMO and LUMO of DES (Bet : Lac = 1 : 4). (d) The HOMO and LUMO of cornin before and after adsorption or elution.

### 3.10. Quantitative comparison with traditional extraction methods

To thoroughly illustrate the advantages of the proposed UA-MSPD method, a detailed quantitative comparison was conducted with several conventional extraction techniques, focusing on critical parameters including extraction time, solvent volume, and estimated energy consumption. As shown in Table S12,<sup>†</sup> the UA-MSPD method dramatically reduced the extraction time by 70–95% compared to maceration, boiling, and ultrasonic extraction.<sup>88–91</sup> Additionally, UA-MSPD utilized significantly smaller amounts of solvent and consumed considerably less energy (approximately  $0.8 \text{ kW h kg}^{-1}$ ) compared to boiling ( $\sim 5.0 \text{ kW h kg}^{-1}$ ) and ultrasonic extractions ( $\sim 2.5\text{--}3.0 \text{ kW h kg}^{-1}$ ). To visually highlight these advantages, a radar chart was generated based on the three key indicators. As shown in Fig. S3,<sup>†</sup> the UA-MSPD method displayed the most favorable overall performance profile, combining minimal solvent use, lower energy input, and exceptionally fast extraction. These results confirm that the UA-MSPD method is not only more efficient but also offers greater economic

returns and environmental sustainability compared to traditional extraction techniques.

## 4. Conclusion

In this research, a highly efficient and eco-friendly extraction technique was proposed in which MOFs and NADESS were synergistically employed for the extraction of active ingredients from *Verbena officinalis* L. The high surface area and porous structure of MOFs enabled them to effectively destroy cell walls, adsorb target components and promote their dissolution when used as adsorbents. Similarly, the abundant hydrogen bond system and adjustable polarity of NADESS enabled them to significantly enhance the solubility of aqueous solutions to active ingredients when used as small additives. UA-MSPD was characterized by the microscale consumption of both samples and solvents, which not only ensured the avoidance of large-scale energy consumption but also enabled a single-step process in which the extraction, sep-

aration, and purification of active ingredients were achieved, thereby significantly simplifying operational procedures. After single factor and response surface optimization, an aqueous solution containing 1.52% NADES (Bet : Lac = 1 : 4) combined with the MOF-199 adsorbent resulted in a total extraction of  $22.99 \pm 0.67 \text{ mg g}^{-1}$  for 5 target substances. Subsequently, four kinds of antioxidant activities of the extracts were tested *in vitro*, and it was found that the antioxidant activity of the extracts was stronger than that of the traditional ethanol crude extract. Additionally, the results of UHPLC-Q-TOF-MS analysis showed that the extract contained 3 iridoids, 4 phenylethanol glycosides and 3 flavonoids. Batch experiments showed the unique role of DESs compared to non-DESs and verified the applicability of the extraction method in different sources of *Verbena officinalis* L. Using DFT calculations, it was found that the  $E_{\text{gap}}$  of the target ingredient was significantly reduced during adsorption and elution, which confirmed the feasibility of the method, and it was found that NADESs could protect the antioxidant active site of the target ingredient through hydrogen bonding so that it could be protected from environmental damage before playing its role, revealing the reason for the high antioxidant activity of the extract. After comparing the degree of fitting, the CatBoost tree model was used to rank the weights of the five influential factors in the extraction process, among which DES dosage was the most important. The GUI model can predict the extraction yield by inputting experimental variables, which provided a basis for further development of the prediction of antioxidant capacity by inputting variables. In summary, this technology was green, economical, and efficient, offering a valuable reference for the enrichment of antioxidant components from other NPs. Furthermore, it demonstrated significant potential for industrial applications, providing robust technical support for enhancing product quality.

## Author contributions

Haixiang Li: writing – original draft, software, project administration and methodology. Kunze Du: writing – review & editing, formal analysis and validation. Chong Liu: software and validation. Yumin Yang: validation. Cailin Ye: software. Xiaoxia Li: project administration and funding acquisition. Yanxu Chang: conceptualization.

## Data availability

The data that support the findings of this study are available from the corresponding author upon reasonable request.

## Conflicts of interest

The authors declare that they have no known competing financial interests or personal relationships that could have appeared to influence the work reported in this paper.

## Acknowledgements

This research was funded by the National Natural Science Foundation of China (Grants No. 82304716 and 82304719), the Tianjin Natural Science Foundation (Grants No. 24JCQNJC00950) and the Special Project for Technological Innovation in New Productive Forces of Modern Chinese Medicines (Grants No. 24ZXZKSY00010). The authors would also like to thank Professor Jun Ren from the North University of China for his help and support with the DFT calculation-related research.

## References

- 1 P. Kubica, A. Szopa, J. Dominiak, M. Luczkiewicz and H. Ekiert, *Planta Med.*, 2020, **86**, 1241–1257.
- 2 R. Nisar, S. Adhikary, S. Ahmad and M. A. Alam, *Molecules*, 2022, **27**, 6329.
- 3 J. Y. Yang, C. S. Guo, L. Su, C. X. Xu, R. T. Li and J. D. Zhong, *Fitoterapia*, 2023, **170**, 105670.
- 4 X. D. Dai, X. D. Zhou, R. Shao, R. P. Zhao, A. K. Yanamandra, Z. M. Xing, M. Y. Ding, J. H. Wang, T. Liu, Q. Zheng, P. Zhang, H. Zhang, Y. Wang, B. Qu and Y. Wang, *Int. J. Mol. Sci.*, 2023, **24**, 7144.
- 5 S. Mukherjee, H. Chopra, R. Goyal, S. H. Jin, Z. Z. Dong, T. Das and T. Bhattacharya, *Discover Nano*, 2024, **19**, 144.
- 6 S. A. A. Shah, N. A. Qureshi, M. Z. Qureshi, S. S. Alhewairini, A. Saleem and A. Zeb, *Saudi J. Biol. Sci.*, 2023, **30**, 103646.
- 7 W. Zhang, P. Zhang, L. H. Xu, K. Gao, J. L. Zhang, M. N. Yao, R. L. Li, C. Guo, J. W. Wang and Q. X. Wu, *Phytomedicine*, 2024, **123**, 155237.
- 8 A. P. Abbott, G. Capper, D. L. Davies, R. K. Rasheed and V. Tambyrajah, *Chem. Commun.*, 2003, 70–71, DOI: [10.1039/b210714g](https://doi.org/10.1039/b210714g).
- 9 J. Cao and E. Z. Su, *J. Cleaner Prod.*, 2021, **314**, 127965.
- 10 S. C. Cunha and J. O. Fernandes, *TrAC, Trends Anal. Chem.*, 2018, **105**, 225–239.
- 11 Y. T. Dai, E. M. Varypataki, E. A. Golovina, W. Jiskoot, G. J. Witkamp, Y. H. Choi and R. Verpoorte, in *Eutectic Solvents and Stress in Plants*, ed. R. Verpoorte, G. J. Witkamp and Y. H. Choi, 2021, vol. 97, pp. 159–184.
- 12 Y. H. Choi, J. van Spronsen, Y. T. Dai, M. Verberne, F. Hollmann, I. Arends, G. J. Witkamp and R. Verpoorte, *Plant Physiol.*, 2011, **156**, 1701–1705.
- 13 C. Ferreira and M. Sarraguca, *Pharmaceuticals*, 2024, **17**, 124.
- 14 J. L. Zuo, P. R. Ma, S. Q. Geng, Y. Z. Kong, X. Li, Z. S. Fan, Y. L. Zhang, A. Dong and Q. Zhou, *J. Sep. Sci.*, 2022, **45**, 717–727.
- 15 S. Bajkacz and J. Adamek, *Talanta*, 2017, **168**, 329–335.
- 16 Y. Chen, D. Yu, Y. Lu, G. Li, L. Fu and T. Mu, *Ind. Eng. Chem. Res.*, 2019, **58**, 7308–7317.
- 17 A. K. El-Deen, *Sep. Purif. Rev.*, 2024, **53**, 100–117.
- 18 L. Ramos, *TrAC, Trends Anal. Chem.*, 2024, **172**, 117601.

- 19 L. Wang, M. Li, Y. Wang, L. Xu, X. He, H. Li and X. Li, *Chem. Eng. J.*, 2024, **496**, 154019.
- 20 L. Xu, X. Zhang, W. Yang, H. Li, J. Wang, L. Wang, X. He, Y. Wang and X. Li, *Chem. Eng. J.*, 2024, **498**, 155224.
- 21 J. K. Wen, H. H. Sun, G. M. Zhang, H. X. Li, H. S. Ren, X. X. Li, J. Li, K. Z. Du and Y. X. Chang, *Ind. Crops Prod.*, 2025, **224**, 120366.
- 22 L.-Q. Peng, Y. Zhang, T.-C. Yan, Y.-X. Gu, X. Zi and J. Cao, *Food Chem.*, 2021, **365**, 130545.
- 23 O. M. Yaghi and H. Li, *J. Am. Chem. Soc.*, 1995, **117**, 10401–10402.
- 24 A. F. Payam, S. Khalil and S. Chakrabarti, *Small*, 2024, **20**, 2310348.
- 25 T. Hurley, V. T. Remcho and K. C. Stylianou, *Chem. – Eur. J.*, 2024, **30**, 202402221.
- 26 R. Q. Xiang, Y. F. Niu, J. Han, Y. L. Lau, H. H. Wu and X. L. Zhao, *RSC Adv.*, 2019, **9**, 33716–33721.
- 27 S. C. Liu, J. M. Pan, Y. Ma, F. X. Qiu, X. H. Niu, T. Zhang and L. L. Yang, *Chem. Eng. J.*, 2016, **306**, 655–666.
- 28 O. A. Salawu, Z. W. Han and A. S. Adeleye, *J. Hazard. Mater.*, 2022, **437**, 129266.
- 29 P. Rajput, S. Yadav, C. Liu and P. Balasubramanian, *J. Water Process Eng.*, 2025, **69**, 106749.
- 30 C. Liu, P. Balasubramanian, J. X. An and F. Y. Li, *npj Clean WaterNpj*, 2025, **8**, 135853.
- 31 H. Li, H. Yue, H. Li, M. Zhu, X. He, M. Liu, X. Li and F. Qiu, *J. Colloid Interface Sci.*, 2025, **680**, 389–404.
- 32 Y. Peng, W. Zhou, X. Cao, M. Liu, H. Zhang, Y. Zhang, Y. Zhou and X. Liu, *Sep. Purif. Technol.*, 2025, **355**, 129797.
- 33 M. Sinkala, N. Mulder and D. Martin, *Sci. Rep.*, 2020, **10**, 1212.
- 34 S. P. Lv, H. Kim, B. B. Zheng and H. Jin, *Appl. Sci.*, 2018, **8**, 582.
- 35 N. Taoufik, W. Boumya, R. Elmoubarki, A. Elhalil, M. Achak, M. Abdennouri and N. Barka, *Mater. Today Chem.*, 2022, **23**, 100732.
- 36 H. J. Zhao, Y. Lyu, J. R. Hu, M. Li, H. Chen, Y. Jiang, M. R. Tang, Y. Wu and W. L. Sun, *Chem. Eng. J.*, 2023, **463**, 142486.
- 37 M. A. Alam, G. Muhammad, M. N. Khan, M. Mofijur, Y. K. Lv, W. L. Xiong and J. L. Xu, *J. Cleaner Prod.*, 2021, **309**, 127445.
- 38 A. Garcia-Roldan, L. Piriou and P. Jauregi, *Front. Plant Sci.*, 2023, **13**, 1072592.
- 39 Z. Z. Fang, Y. F. Li, C. Z. Huang and Q. Q. Liu, *J. Environ. Chem. Eng.*, 2023, **11**, 110155.
- 40 W. Chen, Z. Z. Liu, Y. S. Xie, X. Z. Guo, H. J. Xie, J. H. Chen, Z. Zhang and L. Ding, *Int. J. Biol. Macromol.*, 2025, **298**, 139700.
- 41 Z. N. A. Liu, Y. Li and Y. Y. Teng, *Desalin. Water Treat.*, 2023, **307**, 130–139.
- 42 J. Y. Pan, X. T. Bai, Y. Y. Li, B. H. Yang, P. Y. Yang, F. Yu and J. Ma, *Environ. Res.*, 2022, **205**, 112425.
- 43 L. Ge, W. Zhang, G. Zhou, B. Ma, Q. Mo, Y. Chen and Y. Wang, *Sci. Rep.*, 2017, **7**, 45342.
- 44 A. Z. Kucharska, A. Sokół-Łętowska, J. Oszmiański, N. Piórecki and I. Fecka, *Molecules*, 2017, **22**, 405.
- 45 P.-G. Pietta, *J. Nat. Prod.*, 2000, **63**, 1035–1042.
- 46 C. Liu, P. Balasubramanian, F. Y. Li and H. M. Huang, *J. Hazard. Mater.*, 2024, **480**, 135853.
- 47 I. Gulcin and S. H. Alwasel, *Processes*, 2023, **11**, 2248.
- 48 I. R. Ilyasov, V. L. Beloborodov, I. A. Selivanova and R. P. Terekhov, *Int. J. Mol. Sci.*, 2020, **21**, 1131.
- 49 S. J. Wu, J. H. Wu, L. Z. Xia, C. Chu, D. Liu and M. Gong, *Carbohydr. Polym.*, 2013, **92**, 1612–1614.
- 50 S. Sut, S. Dall'Acqua, K. I. Sinan, G. Zengin, A. I. Uba, O. K. Etienne, S. Jugreet and M. F. Mahomoodally, *J. Sci. Food Agric.*, 2024, **104**, 2820–2831.
- 51 X. Shang, Y. Dou, Y. Zhang, J.-N. Tan, X. Liu and Z. Zhang, *Ind. Crops Prod.*, 2019, **140**, 111724.
- 52 T. Lu and F. Chen, *J. Comput. Chem.*, 2012, **33**, 580–592.
- 53 W. Humphrey, A. Dalke and K. Schulten, *J. Mol. Graphics*, 1996, **14**(33–38), 27–38.
- 54 J. Zhang and T. Lu, *Phys. Chem. Chem. Phys.*, 2021, **23**, 20323–20328.
- 55 T. Lu and Q. Chen, *J. Comput. Chem.*, 2022, **43**, 539–555.
- 56 F. M. Fuad and M. M. Nadzir, *Ind. Crops Prod.*, 2023, **192**, 116069.
- 57 F. M. Fuad and M. M. Nadzir, *J. Mol. Liq.*, 2022, **360**, 119392.
- 58 M. Han, K. Du, X. He, H. Li, J. Li, X. Li and Y. Chang, *Talanta*, 2024, **274**, 125983.
- 59 H. B. Wu, B. Y. Guan, P. He and X.-Y. Yu, *J. Mater. Chem. A*, 2018, **6**, 19338–19341.
- 60 N. M. Mahmoodi and J. Abdi, *Microchem. J.*, 2019, **144**, 436–442.
- 61 H. Zhao, Q. Li, Z. Wang, T. Wu and M. Zhang, *Microporous Mesoporous Mater.*, 2020, **297**, 110044.
- 62 S. Edeballi, *Appl. Surf. Sci. Adv.*, 2023, **18**, 100496.
- 63 E. Biemmi, S. Christian, N. Stock and T. Bein, *Microporous Mesoporous Mater.*, 2009, **117**, 111–117.
- 64 J. Dong, D. Zhao, Y. Lu and W. Y. Sun, *J. Mater. Chem. A*, 2019, **7**, 22744–22767.
- 65 P. Hou, G. Xing, D. Han, Y. Zhao, G. Zhang, H. Wang, C. Zhao and C. Yu, *J. Porous Mater.*, 2019, **26**, 1607–1618.
- 66 Q. Xie, Y. Li, Z. Lv, H. Zhou, X. Yang, J. Chen and H. Guo, *Sci. Rep.*, 2017, **7**, 3316.
- 67 M. Shahsavari, M. Mortazavi, S. Tajik, I. Sheikhsheoie and H. Beitollahi, *Micromachines*, 2022, **13**, 88.
- 68 Z. Ghiamaty, A. Ghaffarinejad, M. Faryadras, A. Abdolmaleki and H. Kazemi, *J. Nanostruct. Chem.*, 2016, **6**, 299–308.
- 69 S. H. Alkandari, J. Lightfoot and B. Castro-Dominguez, *RSC Adv.*, 2023, **13**, 14198–14209.
- 70 G. Li, W. Kujawski, K. Knozowska and J. Kujawa, *RSC Adv.*, 2022, **12**, 29124–29136.
- 71 S. Sanaei-Rad, H. Saeidirosan, B. Mirhosseini-Eshkevari and M. A. Ghasemzadeh, *Res. Chem. Intermed.*, 2021, **47**, 2143–2159.
- 72 S. Salehi, S. Mandegarzad and M. Anbia, *J. Alloys Compd.*, 2020, **812**, 152051.

- 73 E. Buck, S. Lee, L. S. Stone and M. Cerruti, *ACS Appl. Mater. Interfaces*, 2021, **13**, 7021–7036.
- 74 R. G. S. Nair, A. K. N. Nair and S. Sun, *J. Mol. Liq.*, 2023, **389**, 122923.
- 75 S. Zou, C. Wang, J. Li, J. He, X. Gao and Y.-x. Chang, *Sustainable Chem. Pharm.*, 2020, **18**, 100345.
- 76 C. Duan, Y. Yu and H. Hu, *Green Energy Environ.*, 2022, **7**, 3–15.
- 77 Z. Guo, X. Wu, J. Meng, X. Li, Y. Li and L. Hu, *Sep. Purif. Technol.*, 2024, **339**, 126692.
- 78 W. Yang and M. Cao, *Sep. Purif. Technol.*, 2023, **309**, 122957.
- 79 K. Z. Du, J. Li, X. M. Gao and Y. X. Chang, *Sustainable Chem. Pharm.*, 2020, **15**, 100198.
- 80 G. Gygli, X. Xu and J. Pleiss, *Sci. Rep.*, 2020, **10**, 21395.
- 81 L. Lajoie, A.-S. Fabiano-Tixier and F. Chemat, *Pharmaceuticals*, 2022, **15**, 1507.
- 82 S. Mehariya, F. Fratini, R. Lavecchia and A. Zuorro, *J. Environ. Chem. Eng.*, 2021, **9**, 105989.
- 83 X. X. Li and K. H. Row, *Analyst*, 2020, **145**, 2958–2965.
- 84 S. R. Cao, R. Zhu, D. H. Wu, H. T. Su, Z. H. Liu and Z. Q. Chen, *Environ. Pollut.*, 2024, **342**, 123044.
- 85 S. R. Cao, Y. J. Liu, D. W. Ming, J. Tian, J. D. You and Z. Q. Chen, *Environ. Res.*, 2024, **249**, 118356.
- 86 X. He, W. Ji, S. Xing, Z. Feng, H. Li, S. Lu, K. Du and X. Li, *Talanta*, 2024, **268**, 125283.
- 87 J. Ren, L. Zheng, Y. Su, P. Meng, Q. Zhou, H. Zeng, T. Zhang and H. Yu, *Chem. Eng. J.*, 2022, **445**, 136778.
- 88 P. Kubica, A. Kokotkiewicz, M. A. Malinowska, A. Synowiec, M. Gniewosz, S. Hussain, M. Yaqoob, G. K. Bonn, T. Jakschitz, E. A. Mahmoud, T. K. Z. El-Abedin, H. O. Elansary, M. Luczkiewicz, H. Ekiert and A. Szopa, *Antioxidants*, 2022, **11**, 409.
- 89 N. Gibitz-Eisath, M. Eichberger, R. Gruber, C. Seger, S. Sturm and H. Stuppner, *J. Sep. Sci.*, 2020, **43**, 829–838.
- 90 R. Feng, S. Wang, Z. Wang, T. Liu, G. Zhang, S. Xu, T. Ma, X. Lv and L. Zhang, *Biomed. Chromatogr.*, 2024, **38**, e5894.
- 91 K. C. N. Soares, K. E. Pianoski, D. Finger, C. S. Machado, S. P. QuinAia and Y. R. Torres, *An. Acad. Bras. Cienc.*, 2020, **92**, e20181116.